

From alpha to beta ocean

Exploring the role of surface buoyancy fluxes and seawater thermal expansion in setting the upper ocean stratification

Romain Caneill

Doctoral thesis



UNIVERSITY OF GOTHENBURG

Department of Marine Sciences
University of Gothenburg
2023



Dissertation for the Degree of Doctor of Philosophy, Ph.D.,
in Natural Sciences, specialising in Oceanography
University of Gothenburg, 2024

From alpha to beta ocean: Exploring the role of surface buoyancy fluxes and seawater thermal expansion in setting the upper ocean stratification

Romain Caneill, 2023

Except for the appended articles and the figures, this thesis is licensed under a Creative Common Attribution-ShareAlike 4.0 International License (CC BY-SA 4.0)

ISBN 978-91-8069-555-8 (printed)

ISBN 978-91-8069-556-5 (pdf)

Handle <http://hdl.handle.net/2077/79117>

DOI for the sources of this thesis: 10.5281/zenodo.10203249

This book was typeset by the author using L^AT_EX.

Contact: romaincaneill.fr

GPG key fingerprint:

70D5 7116 37B2 9335 9088 F124 D0FE 114E BFFD ED7F

Front cover: Ariane Barba

Back cover photo: The author. Photo credit: Victoria Caneill

Printed by: Stema Specialtyck AB, Borås, 2023

Keywords: Ocean stratification, Thermal expansion coefficient, Buoyancy fluxes, Transition zone, Alpha – beta ocean

Contents

Abstract	i
Sammanfattning	iii
Acknowledgements	v
Funding	vii
Outline	ix
Abbreviations	xi
1 Introduction	1
1.1 Alpha – beta oceans	2
1.2 Thermodynamics of seawater	5
1.3 Buoyancy fluxes, wind, and overturning	6
1.4 The Southern Ocean: a central point of the global circulation	7
1.5 This thesis	8
2 Data and methods	11
2.1 NEMO BASIN	11
2.2 Buoyancy fluxes and Ekman transport of buoyancy	13
2.3 Columnar buoyancy	14
2.4 Stratification Control Index	15
2.5 EN4 and RBF interpolation	16
3 The interplay of buoyancy fluxes and upper ocean stratification	19
3.1 Context	19
3.2 The deep mixing band and its ventilation role	19
3.3 Annual buoyancy fluxes set the position of the PTZ	21
3.4 Balance between seasonal buoyancy loss and stratification sets the DMB	23
3.5 Summary	23
4 The effects of the variable TEC	25
4.1 Context	25
4.2 The TEC dampens the effect of heat fluxes in polar region	27
4.3 The TEC scales the effect of temperature on stratification	28
4.4 Combined effect of the TEC: application to the DMB	30

4.5 Distinguish the effect of the TEC on buoyancy fluxes and on stratification	31
4.6 Summary of the effects of the TEC variations on global scale	32
5 Characterising alpha – beta oceans	33
5.1 Context	33
5.2 Climatologies of the stratification control index	33
5.3 On the link with the mixed layer depth	36
5.4 Summary	37
6 Conclusions and Outlook	39
Bibliography	43

Abstract

The ocean plays a central role in the climate system by absorbing excess anthropogenic heat and carbon dioxide. Moreover, the ocean circulation distributes heat from the tropics towards the poles. Due to the large ocean stratification, vertical exchanges between the ocean interior and the surface are limited. Subduction links the ocean surface and its interior and occurs in winter at mid- or high-latitudes, where the mixed layers (MLs) are deep. In subtropical regions, temperature and salinity decrease below the ML. Temperature has thus a stabilising effect, while salinity has a destabilising effect, a stratification regime called alpha ocean. Opposite, in polar regions, temperature and salinity increase below the ML, and salinity is the stabilising factor, a regime called beta ocean. In between these two regimes lies the polar transition zone (PTZ), where both temperature and salinity are stabilising. Despite the importance of the alpha-beta distinction, the underlying mechanisms controlling these regimes remain unclear. This thesis investigates the factors influencing the upper ocean stratification and the deep MLs adjacent to the PTZs. From observational profiles, we produce novel climatologies of the upper ocean properties. These climatologies confirm that MLs are deep on the poleward flanks of the alpha oceans. Deep MLs are also present in the beta ocean along the coast of Antarctica. In winter, the transition between the different regimes is abrupt. In summer, both temperature and salinity stratify almost the entire ocean. Based on idealised numerical simulations and observations, we find that the buoyancy fluxes largely determine the position of the PTZ. By stabilising the water column poleward of the PTZ, buoyancy fluxes inhibit convection, permitting beta-ocean formation. The exact position of the PTZ and the adjacent deep MLs are determined by the competition between the winter buoyancy loss and the strength of the existing stratification. Importantly, the impact of heat flux on buoyancy is scaled by the thermal expansion coefficient (TEC). The TEC is a strong function of the temperature, a property unique to water. This diminishes the buoyancy fluxes over cold waters. We find that the local value of the TEC in the subpolar region is of paramount importance in controlling the winter buoyancy loss and stratification, and thus the position of the PTZ. A larger TEC value would cause the alpha ocean to extend poleward, inhibiting beta-ocean formation. Considering the importance of the beta ocean in sea-ice formation, the Earth's climate is influenced by the TEC values, which are directly linked to the ocean surface temperature. In summary, this thesis enlightens the central role of the TEC in modulating buoyancy fluxes and thereby controlling the alpha-beta ocean distinction.

Sammanfattning

Havet spelar en central roll i jordens klimatsystem genom att absorbera en del av överskottet av antropogen värme och koldioxid. Dessutom omfördelar havscirkulationen värme från tropikerna till polerna. På grund av havets stora densitetsskiktning är vertikalt utbyte mellan havets yta och de djupare vattenmassorna begränsat. Subduktion är en process som kopplar havsytan till havets inre, vilket sker under vintern på mellan- och höga latituder, där det översta välblandade skiktet (mixed layer, ML) är djupt. I subtropiska hav minskar temperaturen och salthalten under ML. Temperaturen har därmed en stabiliseringseffekt, medan salthalten har en destabiliseringseffekt. Denna skiktregim kallas alphahav. I motsats till detta har polarhavenökande salthalt och temperatur under ML, vilket leder till att salthalten är stabiliseringseffekt. Denna regim kallas betahav. Mellan alpha- och betaregimerna ligger den polara transitionszonen (PTZ), som är en regim där både temperatur och salthalt är stabiliseringseffekter. Trots att distinktionen mellan alpha- och betahav är viktig är de underliggande mekanismerna som kontrollerar dessa regimer inte klarlagda. Denna avhandling undersöker faktorerna som påverkar skiktningen i havets översta del och de djupa ML som återfinns i anslutning till PTZ. Vi använder profiler av salthalt och temperatur från observationer för att producera nya klimatologier av de tre regimerna. Dessa klimatologiska data bekräftar att ML är djupt i den del av alphahaven som ligger närmast polerna. Djupa ML återfinns också i betahavet längs Antarktis kust. Under vintern är övergången mellan de olika regimerna abrupt. Under sommaren bidrar både temperatur- och salthaltsfördelning till skiktningen i nästan hela havet. Baserat på idealiserade numeriska simuleringar och observationer av skiktning och flytkraftsförlöden, finner vi att flytkraftsförlöden till stor del bestämmer positionen för PTZ. Genom att stabilisera vattenpelaren på den sida av PTZ som är närmast polen begränsar flytkraftsförlödena konvektiva processer och tillåter därmed att betahav uppstår. Den exakta positionen av PTZ och de närliggande djupa ML bestäms av en balans mellan förlust av flytkraft under vintern och motståndskraften hos den existerande skiktningen. En viktig faktor är att värmeflödets inverkan på flytkraftsförlödet ändras med värdet på den termiska expansionskoeficienten (TEC). TEC är starkt beroende av vattnets temperatur – en egenskap som är unik för vatten. Denna egenskap leder till minskade flytkraftsförlöden i kallt vatten. Vi finner att det lokala värdet av TEC i den subpolära regionen spelar en mycket viktig roll i att reglera vinterns flytkraftsförlust och stratificering, och därmed positionen för PTZ. Ett högre värdet på TEC skulle orsaka att alphahavet expanderar mot polen och hindrar att betahav bildas. På grund av

betahavets betydelse för bildning av havsis påverkas jordens klimat följaktligen av TEC värdena, som är direkt kopplade till havets yttemperatur. Sammanfattningsvis belyser denna avhandling den centrala roll som TEC spelar i att modulera flytkraftsflöden och därmed i att styra övergången mellan alpha- och betahav.

Acknowledgements

Embarking on this thesis was like navigating the vast and mysterious ocean, following Jules Verne's Captain Nemo in *Vingt mille lieues sous les mers*. Reading this book as a child may have been my first step in earth science. Later, in 2016, my oceanographic expedition set sail in Stockholm with an internship under the guidance of **Fabien Roquet**. **Fabien**, your trust marked the beginning of this adventure. Thank you for not only trusting me during that initial voyage but also inviting me to plunge into the depths once more, this time with greater challenges. I can proudly say that I am an oceanographer now, and this is thanks to you.

Gurvan, your expertise in navigating the NEMO configuration and insightful scientific commentary were like sailing aside a skilled navigator. Thanks, **Jonas**, for all the pertinent comments on manuscripts and all other discussions.

To the crew of friends from Gothenburg University and beyond, thank you. **Etienne**, you showed me the way, and it is always a pleasure to meet you. **Aditya, Anne-Sophie, Benjamin, Birte, Blandine, Doris, Estel, Hanna, Isabelle, James, Jan, Johan, Malin, Martin, Michaela, Milad, Paul, Rickard, Salar, Simon, Solange, Sofia, Stina** (thanks for proofreading the “sammanfattning”), **Theo** (big up for the proofreading of this thesis), **Vincent**, **Yvonne**, and everyone I forgot, our shared lunches, fikas, games, and discussions formed the ports of refuge. I could not imagine finishing this thesis without your camaraderie, support, and laughter.

My gratitude extends to my friends. **Etienne** and **Damien** for the wave surfing in Brittany. **Olivier**, for the mountaineering. **Tim**, for the support. **Tim, Fabien**, and **Vincent** for sharing our passion for music and for the concerts. **Tim** and **Ambroise** for escorting me all the way to my wedding. **Adam** and **Patric** for the climbing and the discovery of Bohuslän’s wonderful climbing spots. Many thanks, **Birte**, for the fikas, dinners, games, and for reading my shitty first drafts. Thanks, **Malin**, for the translation of the “sammanfattning”. Thanks, **Ariane**, for the cover. Tack så mycket **Yvonne** for your hospitality. Tack **Gunnel** and **Karin** for being so warm and for all the good fikas. You are all lighthouses to me.

In the seas of the PhD, the boat is made of thousands of lines of code. The hull has been crafted under the guidance of **Matthieu**. You shared with me your passion for computer science for more than 15 years. Thanks to the precious gift you offered me, I quickly became a good boat carpenter. Sailing is only possible because many people offered their time to chart the way, so thanks to the developers of **Python**, **numpy**, **xarray**, **xgcm**, **matplotlib**, and **La-**

tex. **Matthieu**, I also thank you for opening my eyes to free software, free as in free speech. Apart from moral considerations, they make my life simpler every day. Thanks also to open-source software programs. So thanks to the crews behind **GNU**, **Linux**, **Debian**, **YunoHost**, **Framasoft**, **Nextcloud**, **Trilium**, and many others; without you, my life as a PhD student and as a human would be a mess. I thank everyone I sailed with in this sea of collaborative effort, particularly **Ryan Abernathey**, **Julius Busecke**, **Andrew Barna**, and **Deepak Cherian**. You and many others are paving the way to open source in science; we need to continue! **CodeRefinery**, thanks also for promoting open science and giving me the opportunity to be an exercise assistant in one of your workshops.

As I sailed through the chapters, the creative winds of **Gee** and **Ploum**'s cartoons and blog posts inspired both my personal and academic lives. The melodies of **Indochine** and **Leprous** served as lifeboats during the stormy writing phase. I extend my gratitude by calling on the crews who accompanied my voyage at sea: **Agent Fresco**, **Balthazar**, **Barclay James Harvest**, **Ben Mazu  **, **Bloodhound Gang**, **Edward Elgar**, **Gael Faye**, **Hubert-F  lix Thi  faine**, **Joseph d'Anvers**, **Matmatah**, **Porcupine Tree**, **Supertramp**, **The Alan Parson Project**, and **22**. A journey at sea is not complete without a fair amount of piracy. I hid bottles of Rhum and Beer in this thesis; come find me to get your treasure if you find them! To the pirate lords of metal, **Alestorm**, I raise my bottle of Rhum in gratitude for the good energy. Thanks, **Alexandra Elbakyan**, for the inspiration. Thank you to everyone working to open science and publications. Thanks to the Swedish system for granting me the flexibility to spend valuable time at the harbour during “pappaledig” with my boys. Sweden is one of the few places where it is possible to have children during a PhD without sacrificing family life or the PhD work.

In concluding this acknowledgement, heartfelt thanks to my family. **Manman et Papa** I would not be here today without you pushing me and providing wind in my sails. **Matthieu**, **Ga  lle et Yann**, you are my anchors.

Victoria, **Balthazar**, et **Olivier**, returning home to you after a day of work is like finding a safe harbour. You, my little boys, made me think of something other than science when I came home, whether I wanted it or not. **Victoria** I cannot be grateful enough to you for all the hard work you put into our family, allowing me to rely on you while working. Our couple forms the rock that allows me to navigate the seas of academia with confidence.

Funding

This research was supported by the University of Gothenburg and a travel grant from Adlerbertska stiftelsen.

Outline

This thesis is based on four scientific papers referred to in the text by their roman numerals, as listed below.

List of papers

This thesis is based on the following articles:

- I** Caneill, R., Roquet, F., Madec, G., & Nycander, J. (2022). The Polar Transition from Alpha to Beta Regions Set by a Surface Buoyancy Flux Inversion. *Journal of Physical Oceanography*, 52(8), 1887–1902. <https://doi.org/10.1175/JPO-D-21-0295.1>
- II** Caneill, R., Roquet, F., & Nycander, J. (2023). Southern Ocean deep mixing band emerges from competition between winter buoyancy loss and stratification. *submitted to Ocean Science*. <https://doi.org/10.5194/egusphere-2023-2404>
- III** Caneill, R., & Roquet, F. (2023). Temperature versus salinity: Distribution of stratification control in the global ocean. *in preparation for Ocean Science*
- IV** Roquet, F., Ferreira, D., Caneill, R., Schlesinger, D., & Madec, G. (2022). Unique thermal expansion properties of water key to the formation of sea ice on Earth. *Science Advances*, 8(46). <https://doi.org/10.1126/sciadv.abq0793>

Romain Caneill's contribution

In **Paper I** RC designed the model setup with the help of FR and GM. RC ran all experiments, developed and conducted all analyses. RC was the main contributor for writing the manuscript.

In **Paper II**, RC and all co-authors participated in the design of the study. RC produced all the climatologies and initiated most of the analyses. RC was the main contributor to writing the manuscript.

In **Paper III**, RC produced all climatologies and initiated most of the analyses.

In **Papers I, II, and III**, RC designed and implemented all workflows, allowing for these studies to be reproducible.

In **Paper IV**, RC carried out the analysis of the Estimating the Circulation and Climate of the Ocean (ECCO) product and contributed to the final manuscript.

Other works not included in this thesis:

xgcm xgcm is a Python package that allows for analysis of staggered grid data sets (e.g., model outputs). RC wrote the documentation for using xgcm with the NEMO ocean model. Before this work, no example of using xgcm with NEMO was available.

xnemogcm RC wrote the Python package xnemogcm alone until version 0.4.1 (the latest version is 0.4.2). This package opens NEMO output data and processes them to be used as input for xgcm.

gsw-xarray gsw-xarray is a wrapper around GSW-python for xarray. It adds Climate and Forecast (CF) conventions when existing and adds units to the output. It is also able to convert input variables into the proper unit, if necessary. This project is shared between RC and Andrew Barna (Scripps Institution of Oceanography, UC San Diego).

List of abbreviations

AAIW Antarctic Intermediate Water

ACC Antarctic Circumpolar Current

CB columnar buoyancy

CMIP Coupled Model Intercomparison Project

CO₂ carbon dioxide

CS cooling season

DMB deep mixing band

ECCO Estimating the Circulation and Climate of the Ocean

EOS equation of state

GPCP Global Precipitation Climatology Project

HCC haline contraction coefficient

ISCCP-FH MPF third generation International Satellite Cloud Climatology Project
monthly means

MIMOC Monthly Isopycnal & Mixed-layer Ocean Climatology

ML mixed layer

MLD mixed layer depth

NEMO Nucleus for European Modelling of the Ocean

OAflux Objectively Analyzed Air-Sea Fluxes

OGCM ocean general circulation model

PF Polar Front

PTZ polar transition zone

RBF radial basis function

SAF Subantarctic Front

SAMW Subantarctic Mode Water

SB Southern Boundary

SCI stratification control index

SO Southern Ocean

SSH sea surface height

SST sea surface temperature

TEC thermal expansion coefficient

TKE turbulent kinetic energy

WOCE World Ocean Circulation Experiment

Introduction

More than 50 years ago, pioneering work conducted by Manabe and Wetherald (1967) paved the way to showing the dominant role of carbon dioxide (CO_2) in setting the climate temperature. An increase in CO_2 leads to an increase in the temperature of the atmosphere at the surface of the Earth (Manabe & Wetherald, 1975). This result was found using atmospheric models without any ocean heat transport. However, because of its large heat capacity, the ocean is able to absorb part of the excess heat of the atmosphere (Oeschger et al., 1975; Cess & Goldenberg, 1981). Furthermore, the ocean mitigates atmospheric climate change by absorbing part of the anthropogenic CO_2 (Sabine et al., 2004), concurrently leading to acidification of the ocean (Doney et al., 2009). Moreover, the ocean provides a massive heat and moisture reservoir to the atmosphere, and the oceanic circulation plays a key role in the climate system (Rhines et al., 2008). The exact heat and carbon pathways in the ocean are still not fully understood (Ridge & McKinley, 2021; Gruber et al., 2023).

The global ocean circulation and the vertical fluxes in the ocean are intrinsically linked to the vertical variations of seawater density with depth. The stratification strength is measured by the vertical derivative of density; thus, homogeneous water is unstratified. At the surface, a homogeneous layer called the mixed layer (ML) lies over the pycnocline, where density increases rapidly with depth. By contrast, the deep ocean is weakly stratified. Through its large stratification, the pycnocline blocks vertical mixing, and the result is that the deep ocean is isolated from the atmosphere (Sprintall & Cronin, 2009).

Stratification changes if the density of one layer changes, which can happen by surface buoyancy fluxes, mixing, advection, or diffusion of temperature or salinity (pure “warming” or “freshening”; Bindoff & McDougall, 1994). Another way to change stratification is when isopycnal depth changes without the thermohaline properties changing (“heaving” of isopycnals; Bindoff & McDougall, 1994). Ekman pumping and suction are the processes of water downwelling and upwelling induced by the curl of the wind stress. These adiabatic effects can thus change the upper ocean stratification by heaving.

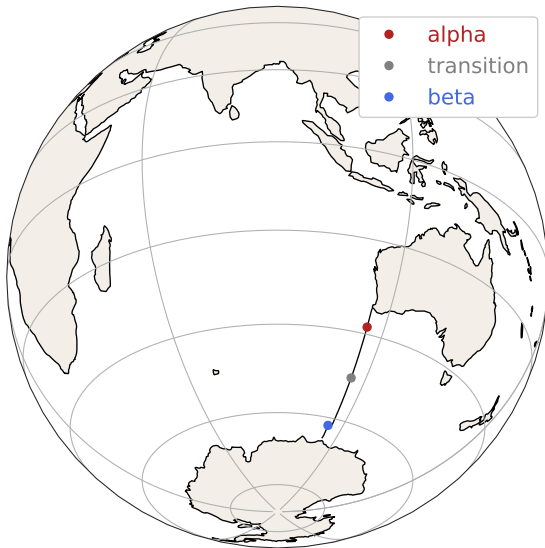


Figure 1.1: Location of the WOCE IO9S transect in the Southern Ocean. The three dots are the location of the profiles in Fig. 1.3. Figure adapted from Caneill and Roquet (2023).

1.1 Alpha – beta oceans

Temperature and salinity in the ocean vary horizontally and vertically. When looking at a transect of temperature and salinity between Australia and Antarctica along the IO9S section defined by the World Ocean Circulation Experiment (WOCE) (Fig. 1.1), two very different regimes are visible (Figs. 1.2 and 1.3). In the subtropical region, close to Australia, the surface temperature is warm (approximately 18°C) and decreases with depth to about 10°C at 400 m deep. Opposite, in the polar region, the near-surface temperature is -1°C and increases with depth to 2°C at 400 m. The transect of Figs. 1.2 and 1.3 has been measured in the summer, so a shallow warm layer occupies the upper 100 meters. The variation of temperature with depth thus follows an opposing pattern in subtropical regions (temperature decreases with depth) compared to polar regions (temperature increases with depth below the winter layer). Salinity follows a similar pattern as temperature: salinity decreases with depth in the subtropics, while in the polar region it increases with depth. These two opposite thermohaline structures have been called alpha and beta oceans by Carmack (2007), representative of subtropical and polar regions, respectively.

The density of seawater decreases with temperature and increases with salinity. Light water always lies above denser water in stable conditions. Thus, when temperature decreases with depth or salinity increases with depth, they contribute to stabilising the water column. Conversely, when temperature increases with depth or salinity decreases with depth, they decrease the stability of the water column. In an alpha ocean, temperature is thus the stabilising component, while salinity tends to decrease stability. It is the opposite in the beta ocean, where salinity is the stratifying component. In between the alpha and beta oceans lies a transition zone, which is usually quite narrow. Here, both temperature and salinity contribute to stability. The progression from al-

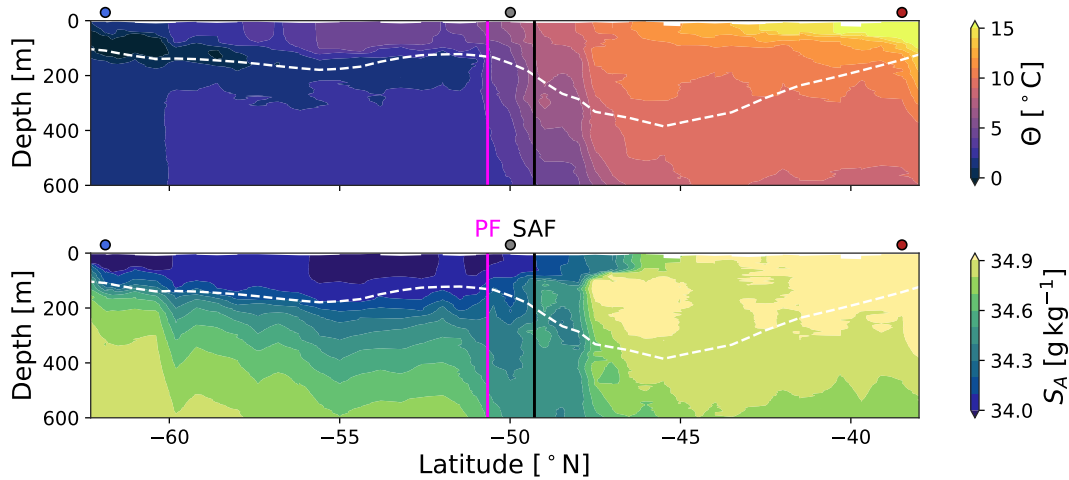


Figure 1.2: Temperature and salinity sections along the IO9S transect. Data are from the hydrographic cruise 09AR20120105 (CCHDO Hydrographic Data Office, 2023). The vertical lines mark the boundaries of, from north to south, alpha ocean, transition zone, and beta ocean. These boundaries are determined by the Subantarctic Front (SAF, black line) and the Polar Front (PF, purple line). The white and dashed line represents the climatological winter mixed layer depth (from de Boyer Montégut (2023)). Figure adapted from Caneill and Roquet (2023).

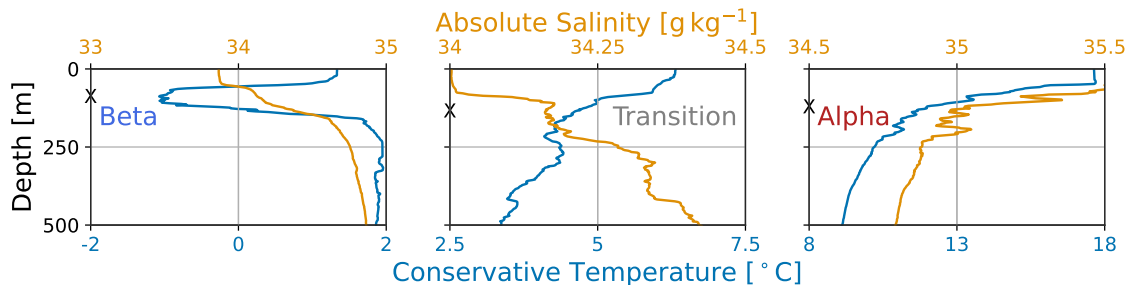


Figure 1.3: Profiles of temperature (blue) and salinity (orange). The three panels correspond to the three dots in Fig. 1.1. The black crosses on the left vertical axes represent the climatological winter mixed layer depth. Figure adapted from Caneill and Roquet (2023).

pha ocean to transition zone to beta ocean, from subtropical to polar regions is a remarkable feature found in the North Atlantic Ocean, the North Pacific Ocean, and the Southern Ocean (SO) (Pollard et al., 2002; You, 2002; Carmack, 2007; Stewart & Haine, 2016). Figure 1.4 presents the distribution of the different zones (adapted from Roquet et al. (2022)).

The alpha – beta distinction has multiple implications. Sea ice can only form if a strong halocline prevents heat-loss-driven convection, a condition found in the beta oceans (Carmack, 2007). At the same time, in the beta oceans, the reservoir of heat located at depth can limit sea-ice growth if the ML reaches this reservoir (Polyakov et al., 2013; Wilson et al., 2019). Sea ice increases the albedo of the ocean and creates feedback on the climate, so a decrease of sea ice in a warmer climate causes a general decrease of the ocean albedo and thus an increase in heat absorption (Curry et al., 1995). Antarctic and

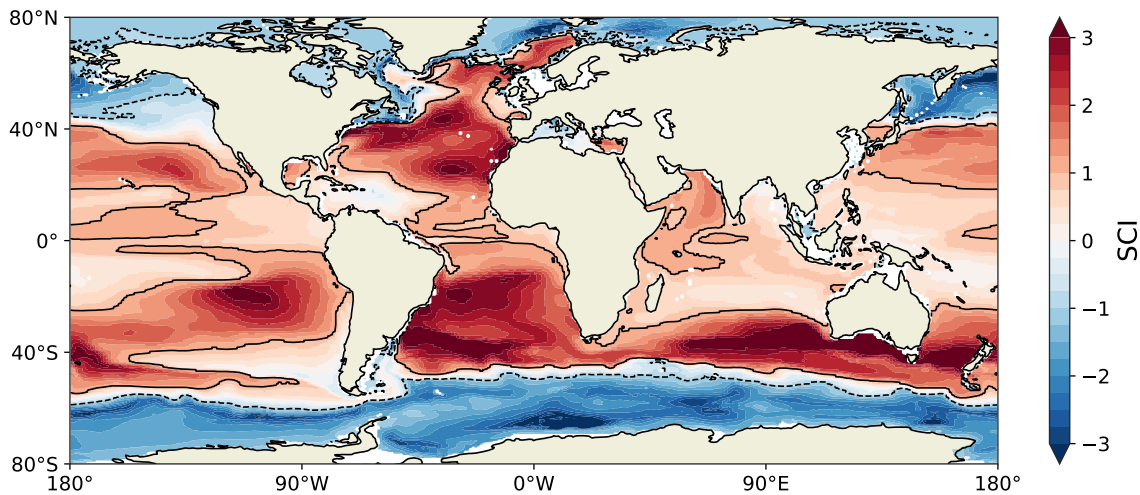


Figure 1.4: Distribution of the alpha oceans (red), beta oceans (blue), and transition zones (light colours). The solid (dashed) lines separate alpha (beta) oceans from transition zones. The zones are determined using the stratification control index below the mixed layer (defined in Chapter 2.4). Figure adapted from Roquet et al. (2022).

Arctic sea-ice extent and properties are changing, and so is the albedo (Perovich & Polashenski, 2012). A decrease in the beta oceans' extent could amplify the decrease in sea ice and, furthermore, amplify the response on the climate system.

The Nordic Seas are situated in a transition zone between the alpha and beta oceans, in which currents and deep water formation are largely impacted by freshwater fluxes (Lambert et al., 2018). Winter MLs are generally deeper in regions stabilised by temperature than when salinity stratifies, which makes the beta ocean able to re-stratify faster (Carmack, 2007). The Barents Sea encounters an increase in heat content induced by the advection of warm water from the Atlantic Ocean, which drives the decrease of sea ice (Årthun et al., 2012; Onarheim et al., 2015). In the Barents Sea, alpha and beta oceans are separated by the Polar Front, which, even if constrained by topography, has intensified since 2005 (Barton et al., 2018). In the global oceans, the transition zones seem to be key places highly sensitive to changes in climate and ocean circulation.

In alpha and beta oceans, when temperature and salinity effects on stratification partially compensate, the water column is subject to double diffusion, a process that contributes to interior mixing (Stern, 1960; Schmitt, 1994; You, 2002). In the transition zone, both temperature and salinity increase the stability; consequently, double diffusion does not occur there.

The permanent halocline characteristic of beta oceans is formed as polar regions encounter more precipitation than evaporation (Carmack et al., 2016; Pellichero et al., 2018). Added to this freshwater excess, the high-latitude ocean loses heat, so the surface temperature becomes cold. The opposite happens in the subtropics, where the ocean evaporates and gains heat, promoting the formation of the thermocline and high surface salinity. Carmack (2007) hypothesised that the thermodynamics of seawater could also play a major role

in the alpha – beta distinction. Yet, the mechanisms behind the alpha – beta distinction remain to be properly described.

1.2 Thermodynamics of seawater

Surface temperature and salinity vary because of, e.g., solar warming, evaporation, sea-ice formation or melt, precipitation, river runoff, and the exchange of heat with the atmosphere. In regions where water sinks to depth and loses contact with the atmosphere, the water masses keep their properties. As the mixing in the ocean interior is reduced compared to the changes induced by surface forcing, these properties are mostly conserved along the way. There are exceptions, such as close to the seafloor, where dissipation of internal waves enhances vertical mixing and thus the consumption of dense, deep water.

At the surface, the combined effects of temperature and salinity set the density of water. At depth, the pressure also impacts the density: while being almost incompressible, seawater density still increases with depth as the pressure becomes very large in the ocean interior. The function giving density from temperature, salinity, and pressure is called the equation of state (EOS). The EOS is a nonlinear relationship. The main nonlinearities arise from the dependence on temperature and pressure.

The temperature-induced nonlinearity makes the thermal expansion coefficient (TEC) vary with temperature and produces the following effect: a variation of 1°C in temperature produces a different variation in density depending on the original temperature. In cold water, the density almost does not change with temperature changes, while it changes a lot in warm temperatures. At low salinities, water can even contract upon warming near the freezing point. Through this effect, when two water parcels with the same density but different compensating temperatures and salinities mix, the resulting water parcel becomes necessarily denser. This effect is called “contraction under mixing”, or cabbeling. The nonlinearity in pressure arises as the effect of temperature on density depends on the pressure (it can also be seen the other way around: the effect of pressure on density depends on temperature). The resulting effect, called thermobaricity, implies that two water parcels having the same density at a certain depth (but different temperature and salinity) will not have the same density as each other when the pressure changes.

Cabbeling and thermobaricity have been recognised as important contributions to interior water mass transformation in the ocean (Garrett & Horne, 1978; McDougall & You, 1990; Iudicone et al., 2008; Klocker & McDougall, 2010; Stewart & Haine, 2016; Groeskamp et al., 2016; Thomas & Shakespeare, 2015). Numerical simulations with modified equations of states have shown that the global circulation and properties are dependent on the used EOS and its nonlinearities (de Boer et al., 2007; Roquet et al., 2015b; Nycander et al., 2015). Rooth (1982), Bryan (1986), and Aagaard and Carmack (1989) pointed out that the decrease in thermal expansion in cold water is likely to enhance the role of salinity in polar regions. While looking at the effect of the EOS on global circulation, this thesis does, however, not focus on cabbeling and

thermobaricity, which are interior mixing processes, but rather on the surface forcing and how it might depend on the TEC.

1.3 Buoyancy fluxes, wind, and overturning

Density of water changes at the surface due to heat and freshwater fluxes. The change in density is quantified by the buoyancy fluxes, which have thermal and haline components coming from heat and freshwater fluxes, respectively. At the surface, for seawater with salinity above 25 g kg^{-1} , the maximum density is always found at the freezing point ($\theta = -1.9^\circ\text{C}$). This means that heat and freshwater gain decrease density (positive buoyancy fluxes). In contrast, heat and freshwater loss increase density (negative buoyancy fluxes). Heat and freshwater fluxes are often compensating as cooling regions tend to receive excess precipitations and vice versa. As a consequence, the buoyancy fluxes are the result of the competition between them (Schmitt et al., 1989).

The ocean is forced at its surface by buoyancy fluxes, which set density, and wind stress, that provides momentum and energy for mixing. The horizontal circulations in the gyres are mainly driven by the curl of wind stress induced by the so-called Sverdrup balance (Sverdrup, 1947; Stommel, 1948; Munk, 1950). However, by changing the density and thus the pressure field, buoyancy fluxes alone can also generate horizontal currents in geostrophic balance (e.g., de Verdière, 1988).

For a long time, buoyancy fluxes along with interior mixing were considered responsible for the overturning circulation in the ocean. Dense waters are formed at high latitudes sink and are consumed by vertical mixing in the interior (Stommel, 1958; Stommel & Arons, 1959; Stommel, 1961; Munk, 1966). However, measurements of vertical diffusivity in the ocean interior were one order of magnitude smaller than the one estimated to consume enough water and produce the observed overturning. Large vertical mixing is enhanced over rough topography and low elsewhere (Polzin et al., 1997).

Later, wind stress driving northward Ekman transport and upward Ekman suction in the SO has been recognised as the driver of an adiabatic overturning cell. The upwelling of water from the ocean interior towards the surface results in the steepening of isopycnals. Mesoscale eddies tend to flatten the isopycnals and counteract the effect of wind. Wind is thus considered the main driver of the upper cell of the overturning circulation (e.g., Toggweiler & Samuels, 1998; Wolfe & Cessi, 2010; Cessi, 2019). However, on the complete opposite view, numerical experiments have shown that in the presence of a reentrant channel, buoyancy fluxes alone could drive overturning and deep stratification (Barkan et al., 2013; Sohail et al., 2019; Klocker et al., 2023b).

In all cases, the SO is a central place for setting the general circulation. The next section describes this ocean.

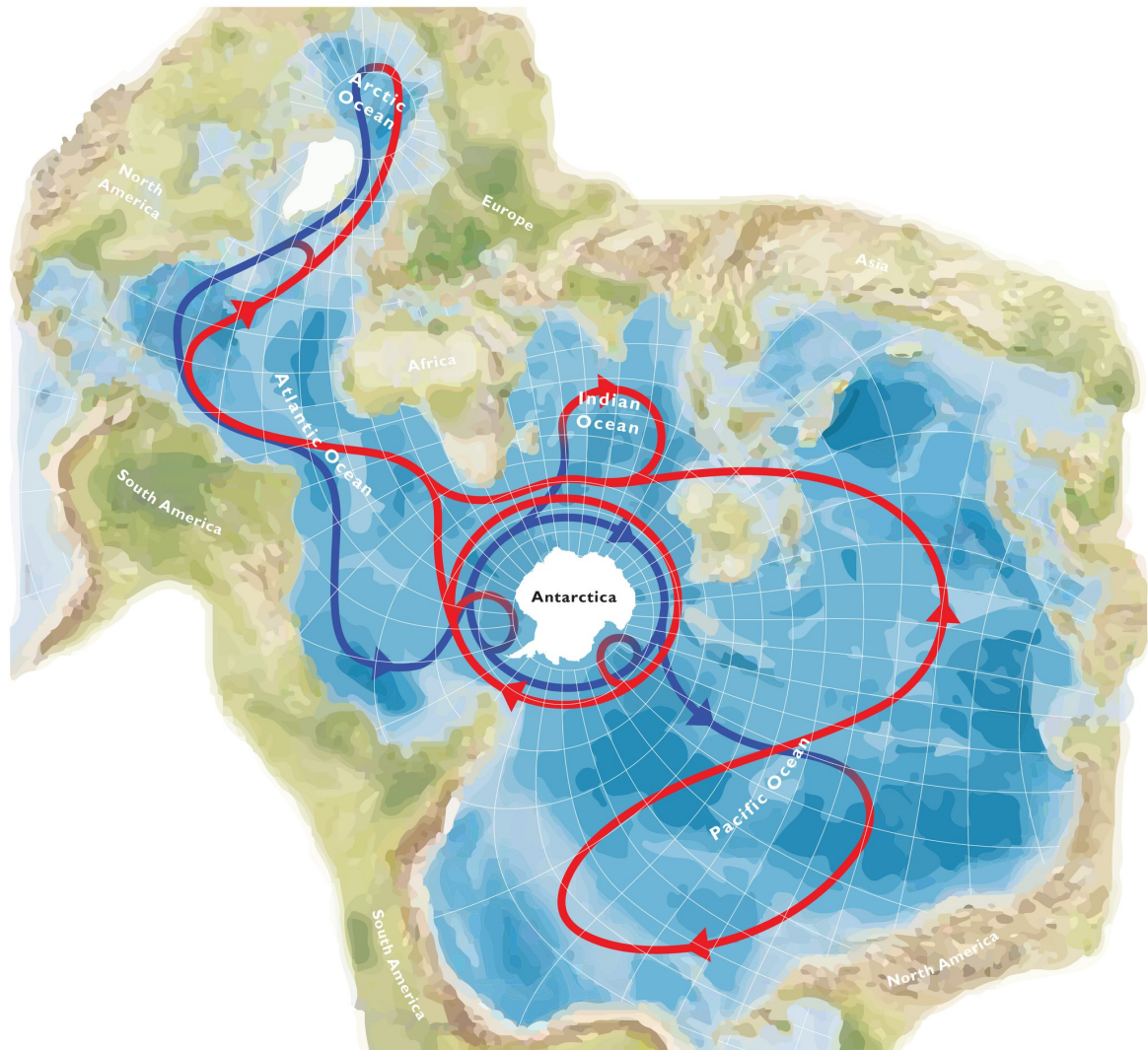


Figure 1.5: Spilhaus projection of the world oceans. The arrows represent a highly simplified view of the global overturning circulation, with surface currents in red and deep currents in blue. The Southern Ocean appears to connect the Atlantic, Pacific, and Indian basins. Figure from Meredith (2019).

1.4 The Southern Ocean: a central point of the global circulation

The SO connects the three major basins of the global ocean: the Atlantic, Indian, and Pacific Oceans. This connection is best seen in the Spilhaus projection of the Earth's oceans, where it appears that all oceans are large water pools connected through the SO (Fig. 1.5, from Meredith (2019)). Each ocean has its own thermohaline properties, so these properties become linked through the SO.

The SO hosts the Antarctic Circumpolar Current (ACC), the world's largest oceanic current. The ACC flows without a meridional boundary blocking it and has a transport of about 135 Sv at the Drake passage (Cunningham et al., 2003). The ACC is zonally organised into fronts. These fronts have been historically

defined based on hydrographic properties (e.g., Emery, 1977; Whitworth, 1980), such as the geographical position of a certain isotherm at a certain depth (Belkin & Gordon, 1996). These fronts are thus defined as the boundaries of different water masses. Other definitions exist; instead of using a property, one can use a gradient, refining the idea of a boundary between water masses. With the era of satellite observations of sea surface height (SSH), other definitions arose, where fronts are defined as dynamical fronts, i.e., they correspond to the location of the jets that form the ACC. Indeed, horizontal gradients of SSH are directly linked to surface velocities through geostrophy. The two main fronts of interest in this thesis are the Subantarctic Front (SAF) and the Polar Front (PF). The SAF is closely linked to the northern boundary of the ACC, although its definition varies among the authors that define dynamic fronts. North of the SAF, deep MLs are found in winter, where the Subantarctic Mode Water (SAMW) originates. South of the SAF, a salinity minimum is found at depth, a marker specific for the Antarctic Intermediate Water (AAIW). The PF marks the northern extent of the cold Antarctic Surface Water. The SAF and PF indicate the boundary between alpha – transition and transition – beta, respectively (Pollard et al., 2002; Pauthenet et al., 2017).

The SO not only hosts a vigorous horizontal current but is also a key area of formation of intermediate and deep water, playing an important role in the global overturning circulation. Antarctic Bottom Water is mostly produced close to the coast of Antarctica, where sea ice is formed, producing dense, cold, and salty water that flows down to the bottom of the ocean. Intermediate waters consist of SAMW and AAIW and form the upper limb of the overturning circulation. These waters are formed north of the SAF and between the SAF and PF, respectively. MLs that are deeper than 250 m north of the SAF form the deep mixing band (DMB) (Dong et al., 2008; DuVivier et al., 2018). In winter, intense heat loss and the Ekman transport of cold water deepen the ML (Naveira Garabato et al., 2009; Holte et al., 2012; Rintoul & England, 2002). The SAMW originates from these deep MLs and reaches the permanent pycnocline through lateral advection (Belkin & Gordon, 1996; Speer et al., 2000; Hanawa & Talley, 2001; Sallée et al., 2010; Klocker et al., 2023a).

1.5 This thesis

We have seen that the boundaries between subtropical and subpolar regions, particularly in the SO, are central to the global circulation in the oceans and the climate. As the EOS is nonlinear, the effect of temperature on stratification and the effect of heat fluxes on buoyancy fluxes are not the same depending on the water temperature and, thus, depending on the region. The type of stratification is similar in all the polar regions, and the transition between alpha and beta is linked to intermediate water formation. The aim of this thesis is to assert the role of the local value of the TEC in modulating buoyancy fluxes and stratification strength, and thus to understand how this intrinsic property of seawater controls part of the large-scale state of the oceans. This thesis also contributes to the understanding and description of the SO fronts from

the perspective of stratification regimes. Finally, this thesis provides a general description of the alpha, beta, and transition zones in the global ocean.

We use a combination of numerical simulations in which we modify the EOS to assess the role of the TEC and how changing the buoyancy fluxes of thermal stratification modify the circulation and state of the ocean. We also combine observational data to produce climatologies of stratification (strength and regime) and buoyancy fluxes, which allows us to describe the processes from which the DMB and transition zones are arising.

Chapter 2 briefly describes the data and methods used in this thesis; more detailed descriptions are found in the attached papers. Based on **Papers I and II**, Chapter 3 presents how the interplay between buoyancy fluxes and summer stratification sets the winter stratification. Chapter 4 provides a summary of the major role of the local value of the TEC in shaping the ocean state, using **Papers I, II, and IV**. The global description of the stratification regimes is done in Chapter 5 (**Paper III**). Finally, conclusions and perspectives are given in Chapter 6.

Data and methods

2.1 NEMO BASIN (Paper I)

This section presents the numerical model configuration used in **Paper I**. The reader is referred to the paper for all details. The Nucleus for European Modelling of the Ocean (NEMO) (Madec, 2019) ocean general circulation model (OGCM) is used to assess the role of surface buoyancy fluxes on the type of stratification of the subpolar regions.

The configuration represents an idealised basin with a size of 40° of longitude and 60° of latitude, with its southern boundary at the equator. A 1° longitude Mercator grid is used, and the topography is defined as slopes (Fig. 2.1a). To better represent the western boundary currents, we use a terrain following coordinate with 36 vertical levels, which allows the currents to adjust their vorticity by going up or down the boundary slope. The topography is flattened around the equator to minimise ageostrophic currents induced by the numerical schemes. No wall is present at the equator, but a no-meridional flux condition is applied. The turbulent kinetic energy (TKE) closure is used, with a background diffusivity of $10^{-4} \text{ m}^2 \text{ s}^{-1}$.

Heat and freshwater fluxes are represented using relaxation laws, so that analytical functions for the restoring values of temperature and salinity are provided. The heat flux is split into penetrative (solar) and non-penetrative components. The wind stress is zonally constant, with no meridional component. These forcing fields are inspired by Lévy et al. (2010) and Wolfe and Cessi (2014) and represent zonal averages over the ocean (Fig. 2.1).

Due to the low resolution of the configuration, it can be run for 2000 years until equilibrium is reached. The last 50 years are used for the analyses, either as global time averages or monthly averages.

A novelty of these simulations is the use of the simplified equation of state (EOS) proposed by Roquet et al. (2015b) (Eq. (2.1)). The thermal expansion coefficient (TEC), α , is linearly dependent on temperature and pressure (Eq. (2.2)), while the haline contraction coefficient (HCC), β , is constant (Eq. (2.3)).

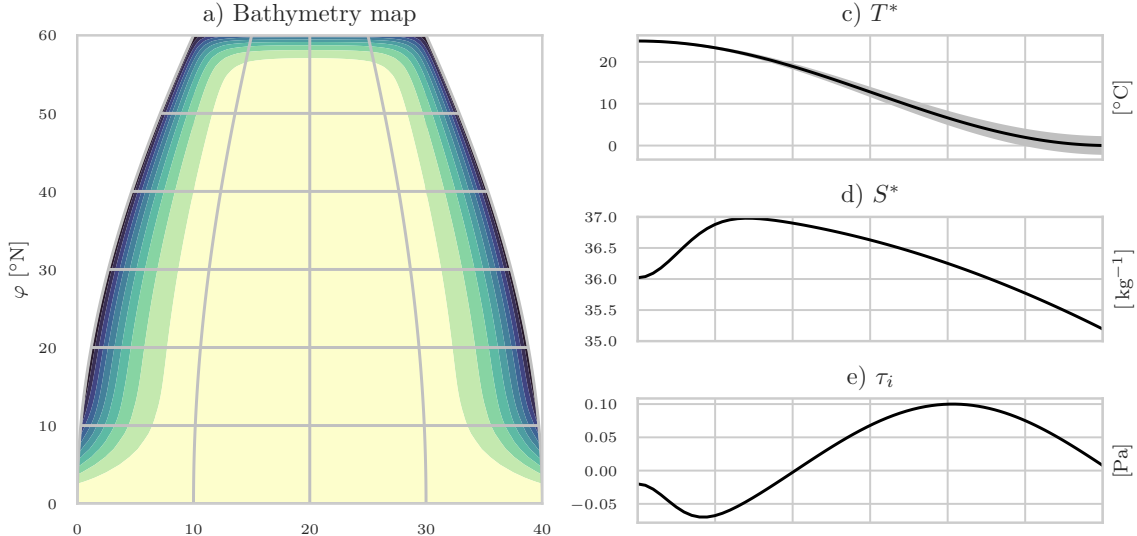


Figure 2.1: Bathymetry of the basin in a) and b). Forcing fields used by the model, with c) the restoring temperature, d) the restoring salinity, e) the zonal wind stress. The average values are plotted in black. For panels c), the gray zone represents the seasonal variations. Figure adapted from Caneill et al. (2022).

Coefficient	Value	Description
a_0	$1.65 \times 10^{-1} \text{ }^{\circ}\text{C}^{-1} \text{ kg m}^{-3}$	linear thermal expansion coefficient
b_0	$7.6554 \times 10^{-1} (\text{g/kg})^{-1} \text{ kg m}^{-3}$	linear haline expansion coefficient
C_b	$9.9 \times 10^{-3} \text{ }^{\circ}\text{C}^{-2} \text{ kg m}^{-3}$	cabbeling coefficient
T_h	$2.4775 \times 10^{-5} \text{ }^{\circ}\text{C}^{-1} \text{ dbar}^{-1} \text{ kg m}^{-3}$	thermobaric coefficient

Table 2.1: Default value of the simplified equation of state coefficients.

This allows us to adjust buoyancy fluxes and stratification by changing the parameters of the TEC, a_0 and C_b :

$$\rho(\Theta, S_A, p) = \rho_0 - \left(a_0 + \frac{1}{2} C_b \Theta_a + T_h p \right) \Theta_a + b_0 S_a \quad (2.1)$$

$$\alpha = \frac{1}{\rho_0} (a_0 + C_b \Theta_a + T_h p) \quad (2.2)$$

$$\beta = \frac{b_0}{\rho_0} \quad (2.3)$$

with $\Theta_a = \Theta - 10 \text{ }^{\circ}\text{C}$, $S_a = S_A - 35 \text{ g kg}^{-1}$, and p the pressure.

Five combinations of parameters are used to test the sensitivity of stratification to annual buoyancy fluxes (Table 2.2).

Name	a_0 in $^{\circ}\text{C}^{-1} \text{kg m}^{-3}$	C_b in $^{\circ}\text{C}^{-2} \text{kg m}^{-3}$
ref	1.65×10^{-1}	9.9×10^{-3}
A	1.65×10^{-1}	13.2×10^{-3}
B	1.45×10^{-1}	8.7×10^{-3}
C	1.85×10^{-1}	11.1×10^{-3}
D	1.65×10^{-1}	6.6×10^{-3}

Table 2.2: The five combinations of parameters.

2.2 Buoyancy fluxes and Ekman transport of buoyancy (Papers I and II)

Surface buoyancy fluxes are an essential component of global circulation, as they modify water density. Thus, they are calculated both for the model simulations and from observations. They are derived from heat and freshwater fluxes (e.g., Gill & Adrian, 1982):

$$\mathcal{B}^{surf} = \underbrace{\frac{g\alpha}{\rho_0 C_p} Q_{tot}}_{\mathcal{B}_{\Theta}^{surf}} - \underbrace{\frac{g\beta S}{\rho_0} (E - P - R)}_{\mathcal{B}_S^{surf}} \quad (2.4)$$

where g is the gravitational acceleration, $C_p \simeq 3997 \text{ J kg}^{-1} \text{ K}^{-1}$ the heat capacity of seawater, Q_{tot} the total heat flux in W m^{-2} , E the evaporation, P the precipitation, R the river runoff all in $\text{kg m}^{-2} \text{ s}^{-1}$, and S the surface salinity. The buoyancy fluxes \mathcal{B}^{surf} are in $\text{m}^2 \text{ s}^{-3}$. Buoyancy fluxes are heat and freshwater fluxes scaled by α and β , respectively.

In **Paper I**, heat and freshwater fluxes are outputs of the NEMO simulations. In **Paper II**, we used observations based on a mixture of different products to compute the heat and freshwater fluxes in the Southern Ocean (SO). The Objectively Analyzed Air-Sea Fluxes (OAflux) 1-degree dataset (Yu & Weller, 2007) provides turbulent heat fluxes and evaporation. The third generation International Satellite Cloud Climatology Project monthly means (ISCCP-FH MPF) provides radiative fluxes (Schiffer & Rossow, 1983; Rossow & Schiffer, 1999). The Global Precipitation Climatology Project (GPCP) Version 2.3 provides precipitation (Adler et al., 2018). We used river runoff from Estimating the Circulation and Climate of the Ocean (ECCO) Version 4, Release 4 (Forget et al., 2015). The reader is referred to **Paper II** for a more detailed description of the datasets used. Due to the difficulties of computing turbulent fluxes, following Schanze and Schmitt (2013), we removed the global average (time, longitude, and latitude) of the heat and freshwater fluxes to get a balance. We then define a cooling season (CS) from April to September in the SO for estimating the buoyancy loss.

The Ekman transport advects cold and fresh water northward in the SO; this

effect is taken into account by calculating the Ekman transport of buoyancy:

$$\mathcal{B}_{\Theta}^{Ek} = -\frac{g\alpha}{\rho_0 f} \left(\tau^y \frac{\partial \Theta}{\partial x} - \tau^x \frac{\partial \Theta}{\partial y} \right) \quad (2.5)$$

$$\mathcal{B}_S^{Ek} = \frac{g\beta}{\rho_0 f} \left(\tau^y \frac{\partial S}{\partial x} - \tau^x \frac{\partial S}{\partial y} \right) \quad (2.6)$$

with τ^x and τ^y the eastward and northward wind stress, respectively, and f the Coriolis parameter. The fluxes $\mathcal{B}_{\Theta}^{Ek}$ and \mathcal{B}_S^{Ek} are contained within the Ekman layer. When making the commonly used assumption that the Ekman layer is entirely contained within the mixed layer (ML), the total buoyancy flux, $\mathcal{B} = \mathcal{B}^{Ek} + \mathcal{B}^{surf}$, is the buoyancy flux to the ML. We used daily averages from the CMEMS “Global Ocean Wind L4 Reprocessed 6 Hourly Observations” for wind stress and ARMOR3D weekly product (Guinehut et al., 2012) for computing temperature and salinity gradients.

2.3 Columnar buoyancy (Paper II)

We use columnar buoyancy (CB) as an indicator of stratification strength (Lascaratos & Nittis, 1998; Herrmann et al., 2008):

$$CB(Z) = \int_Z^0 -z N^2(z) dz \quad (2.7)$$

with the z-axis oriented upward, Z the depth at which the CB is computed, and $N^2(z) = -\frac{g}{\rho_0} \frac{\partial \tilde{\rho}_\theta}{\partial z}$ the squared buoyancy frequency. $\tilde{\rho}_\theta$ is the locally referenced potential density (Vallis, 2017). In our case, using potential density reference at the surface instead of locally referenced potential density to compute $N^2(z)$ leads to negligible differences. This way, the formula can be expressed by using density profiles instead of doing two numerical operations (differentiation followed by summation). Integration by parts of Eq. (2.7) then gives:

$$CB(Z) \simeq \frac{g}{\rho_0} \int_Z^0 [\rho_\theta(Z) - \rho_\theta(z)] dz \quad (2.8)$$

The CB is positive in a stable stratification. It represents the amount of buoyancy that must be lost to produce a ML of depth Z and of potential density $\rho_\theta(Z)$. Dividing it by a time gives the buoyancy flux that must be applied during this time to form this ML, called B_Z (Faure & Kawai, 2015). We only consider B_Z to the depth of 250 m (i.e., B_{250}), which is the threshold for defining deep ML used by DuVivier et al. (2018):

$$B_{250} = \frac{-CB(-250)}{\Delta t} \quad (2.9)$$

The ocean loses buoyancy during six months of the year, so to allow a direct comparison between the mean buoyancy loss and stratification, we took six months for Δt .

B_{250} can be split into the thermal and haline components to quantify their individual effects:

$$B_{250} = \underbrace{\frac{g}{\Delta t} \int_{-250}^0 \alpha(z) \frac{\partial \Theta}{\partial z} z dz}_{B_{250}^\Theta} - \underbrace{\frac{g}{\Delta t} \int_{-250}^0 \beta(z) \frac{\partial S}{\partial z} z dz}_{B_{250}^S} \quad (2.10)$$

In **Paper II**, B_{250} is computed using the Monthly Isopycnal & Mixed-layer Ocean Climatology (MIMOC) in depth coordinates produced by Schmidtko et al. (2013).

2.4 Stratification Control Index (Papers I, III, and IV)

To compare the relative impact of temperature and salinity on stratification strength, we define the stratification control index (SCI):

$$SCI = \frac{N_\Theta^2 - N_S^2}{N_\Theta^2 + N_S^2} \quad (2.11)$$

$$N^2 = -\frac{g}{\rho_0} \frac{\partial \rho_\Theta}{\partial z} = N_\Theta^2 + N_S^2 \quad (2.12)$$

$$N_\Theta^2 = g\alpha \frac{\partial \Theta}{\partial z} \quad (2.13)$$

$$N_S^2 = -g\beta \frac{\partial S_A}{\partial z}. \quad (2.14)$$

N_Θ^2 and N_S^2 are the thermal and haline components of the squared buoyancy frequency N^2 . A negative value of N_Θ^2 (N_S^2) means that temperature (salinity) has a destabilising effect. We only consider stable stratification ($N^2 > 0$), so if temperature or salinity has a destabilising effect, it means that the other property compensates and has a larger stratifying effect. The SCI is the tangent of the Turner angle ($SCI = \tan(Tu)$) (Ruddick, 1983).

The SCI catches states of no temperature or no salinity stratification:

$$N_\Theta^2 = 0 \implies SCI = -1 \quad (2.15)$$

$$N_S^2 = 0 \implies SCI = 1 \quad (2.16)$$

Thus, temperature has a stratifying effect when $SCI > -1$. Salinity follows a symmetrical pattern and stratifies when $SCI < 1$. We can define three zones bounded by $SCI = \pm 1$ and characterised by different thermohaline stratification regimes. We use these three zones for the definition of alpha ocean, transition zone, and beta ocean:

- *alpha ocean* when $1 < SCI$,
- *transition zone* when $-1 \leq SCI \leq 1$,
- *beta ocean* when $SCI < -1$.

The SCI can be computed at any depth below the ML, but as we mainly focus on the permanent pycnocline, we compute the SCI just below the winter ML. In the definition that Carmack (2007) proposed, alpha (beta) means that temperature (salinity) stratifies. According to this definition, the $-1 \leq SCI \leq 1$ region would thus be both alpha and beta. Stewart and Haine (2016) proposed a definition of the transition zone based on the Turner angle at each location and date. Their transition zones are defined as where the stratification seasonally evolves between being mainly stratified by temperature and being mainly stratified by salinity. “Transition” is thus to be understood as “alternating” for them, while in our definition, “transition” means “doubly stratified”, in contrast to the alpha and beta oceans where a partial compensation occurs between temperature and salinity.

In **Papers I and IV** the SCI has been computed from the models’ monthly outputs (NEMO BASIN and ECCO) and in **Paper III** it has been computed on each individual profile of the EN4 database (Sect. 2.5).

2.5 EN4 and radial basis function interpolation (Paper II)

Paper III uses the EN.4.2.2 (Good et al., 2013) ensemble members using Gouretski and Cheng (2020) MBT and Gouretski and Reseghetti (2010) XBT corrections. To remove spikes prior to computing the vertical gradient, the profiles have been smoothed and re-sampled to a regular vertical grid (Johnson et al., 2002) (more details are given in **Paper III**).

The mixed layer depth (MLD) is computed using a density threshold criteria of 0.03 kg m^{-3} referenced to 10 m depth (de Boyer Montégut, 2004). The SCI is then computed using the temperature and salinity values at 10 m and 30 m under the ML. The MLD and SCI are then gridded onto a regular longitude – latitude grid for each month using a radial basis function (RBF) interpolation. The class *scipy.interpolate.RBFInterpolator* from the Python *scipy* library is used (Virtanen et al., 2020).

To account for the anisotropy between the longitude and latitude scale factors, the latitude (φ) is transformed by a Mercator projection, using the following formula:

$$\varphi' = \ln\left(\tan\left(\frac{\varphi}{2}\frac{\pi}{180} + \frac{\pi}{4}\right)\right) \cdot \frac{180}{\pi} \quad (2.17)$$

This will virtually increase the difference in latitude between two points located in polar regions, so that longitude and latitude become isotropic.

To find a balance between accuracy and computation efficiency, the closest 300 points around each grid point are selected for the interpolation using the distance d :

$$d^2 = \left[\frac{\Delta\lambda}{L_\lambda}\right]^2 + \left[\frac{\Delta\varphi'}{L_{\varphi'}}\right]^2 + \left[\frac{\Delta t}{L_t}\right]^2 \quad (2.18)$$

with $\Delta\lambda$ the difference of longitude between the grid point and the measurement point, $\Delta\varphi'$ the difference of modified latitude, and Δt the number of days of difference between the measurement and the interpolation date. The three L s express the decorrelation scales for longitude (L_λ), modified latitude ($L_{\varphi'}$) and

time (L_t). The three decorrelation scales have been chosen as: $L_\lambda = L_{\varphi'} = 3.3^\circ$, and $L_t = 45$ d, similar to the coefficient used to produce the MIMOC database (Schmidtko et al., 2013). We used a Gaussian function for the interpolation kernel.

Chapter 3

The interplay of buoyancy fluxes and upper ocean stratification key to formation of deep mixed layers (Papers I and II)

3.1 Context

At the surface of the ocean, fluxes of heat and freshwater induce a change in density, and they can thus be converted into buoyancy fluxes. Winter surface buoyancy loss due to heat produces dense water in the Nordic Seas (Isachsen et al., 2007; Petit et al., 2020) and deepens the mixed layer (ML) in the Southern Ocean (SO), producing Subantarctic Mode Water (SAMW), a process further enhanced by Ekman transport of cold water (Naveira Garabato et al., 2009; Holte et al., 2012; Rintoul & England, 2002). On the other hand, an increase in freshwater fluxes can dampen the formation of intermediate or deep water, as in the Labrador Sea (Lazier, 1980).

Buoyancy fluxes impact the transformation of water masses (Walsh, 1982; Speer et al., 2000; Kuhlbrodt et al., 2007; Cessi, 2019), as well as the rate of formation of deep water in the North Atlantic basin (Mauritzen & Häkkinen, 1999). Water mass transformations can arise from surface buoyancy fluxes but also from diffusive or advective fluxes. In subpolar to polar regions, heat is lost in winter and freshwater is gained from precipitations. This is thus a balance between these two components that sets the final buoyancy fluxes (Schmitt et al., 1989). Moreover, both haline and thermal components of buoyancy fluxes must be studied separately in water mass transformation studies (Speer et al., 1995; Karstensen & Lorbacher, 2011).

3.2 The deep mixing band and its ventilation role

In winter in the SO, a belt of MLs deeper than 250 m is located north of the Subantarctic Front (SAF) (Fig. 3.1 and Dong et al. (2008)). The belt

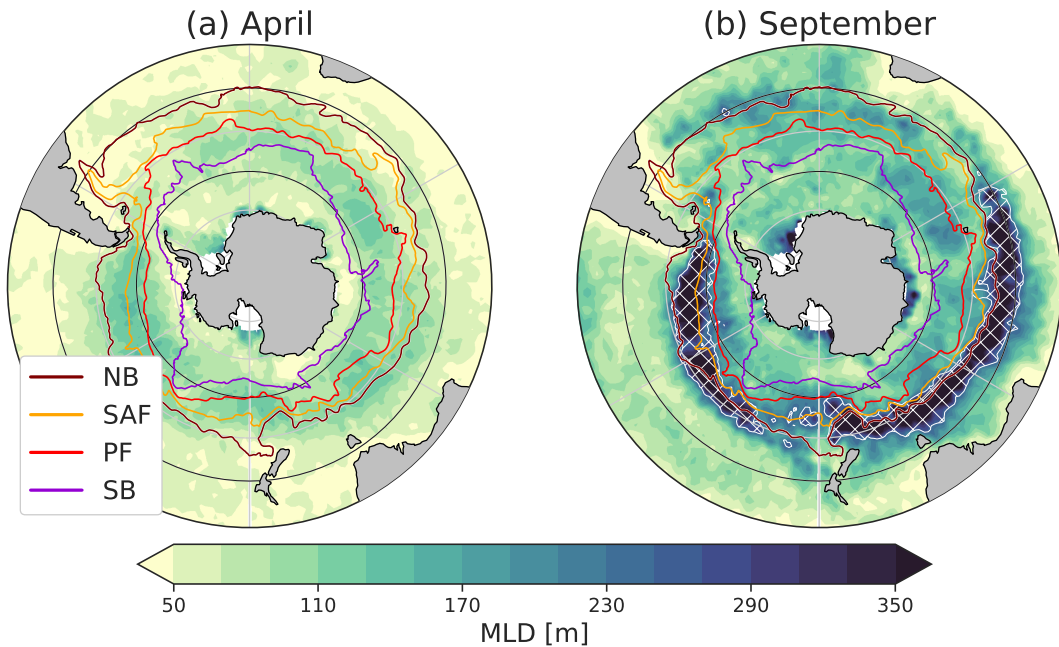


Figure 3.1: Climatology of the mixed layer depth in the Southern Ocean in (a) April and (b) September. The area hashed in white represents the deep mixing band, where the mixed layers are deeper than 250 m. The main fronts of the Southern Ocean are also plotted. The mixed layer depths are from de Boyer Montégut (2023) and the fronts from Park et al. (2019). Figure adapted from Caneill et al. (2023).

is referred to as the deep mixing band (DMB) (DuVivier et al., 2018). The DMB is important for the global stratification structure of the ocean, as the SAMW is formed when water escapes the DMB by lateral induction (Belkin & Gordon, 1996; Speer et al., 2000; Hanawa & Talley, 2001; Klocker et al., 2023a). SAMW is thus formed through a mixture of air-sea fluxes and Ekman transport (Sloyan & Rintoul, 2001). SAMW takes up a large amount of anthropogenic carbon dioxide (CO_2) (Sabine et al., 2004), so it is important to understand the processes of its formation. SAMW constitutes a significant part of the upper limb of the global overturning circulation and thus is able to transport its properties (CO_2 , heat, etc) to depth (Sloyan & Rintoul, 2001). The DMB is found in the Indian and Pacific sectors of the SO. It has been found that winter heat loss is the main driver of ML deepening within the DMB and that the transport of cold water by Ekman transport intensifies buoyancy loss (Naveira Garabato et al., 2009; Holte et al., 2012; Rintoul & England, 2002). However, the question of why it is so narrow is still not fully answered, and any unique component of surface forcing is not able to explain it (e.g., wind stress, wind stress curl, buoyancy flux, or mesoscale eddy activity) (DuVivier et al., 2018).

3.3 Annual buoyancy fluxes set the position of the polar transition zone (Paper I)

In **Paper I**, our idealised simulations (Chapter 2.1) are able to reproduce an ocean with two different stratification types: alpha in the subtropics and beta in the polar region. The alpha – beta boundary is oriented along a north-east diagonal (**Paper I**, Fig. 5c) and is similar to the North Atlantic polar transition zone (PTZ). A single region of convection is present, as only one hemisphere was represented. This region of deep MLs is located on the northern flank of the alpha ocean and contains the densest surface water. The deepest MLs reach the bottom, as no denser water is present. As these dense waters are formed between the subtropical and subpolar gyres, they are equivalent to the mode and intermediate waters of the SO. In the beta ocean, the winter ML is shallower than 200 m due to the large stratification induced by freshwater.

Deep MLs are formed in a region of annual buoyancy loss, and the beta ocean is encountering annual buoyancy gain. This buoyancy gain comes from positive freshwater fluxes having a greater effect than heat loss on buoyancy fluxes. By changing the equation of state (EOS) as a way to change the relative importance of freshwater and heat on buoyancy fluxes, we show that the transition between the alpha and beta oceans is located close to the position where the sign of the annual buoyancy fluxes changes. Moreover, convection occurs systematically on the northern flank of the alpha ocean and is thus bounded to the north by the PTZ. A schematic view of the process leading to the formation of the transition is drawn in Figure 3.2. After leaving the subtropics, surface water that flows poleward within the western boundary current enters a region of annual buoyancy loss driven by intense heat loss. Along its way, the ML deepens until the water enters a region of annual buoyancy gain. In this region, the ML becomes shallower, and a freshwater cap is able to build up, preventing convection from occurring. The intermediate water formed in the deep ML region is then advected equatorward, although it is also associated with a cyclonic flow in the north before flowing equatorward at the western boundary at depth.

The buoyancy gain in beta ocean is driven by positive freshwater fluxes, while the thermal component of buoyancy fluxes becomes small. The thermal component becomes small not because of a reduction of heat fluxes but, on the contrary, because of the decrease in the thermal expansion coefficient (TEC) in cold water. Chapter 4 describes our findings on the impact of TEC variations on global ocean circulation and climate.

The wind forcing was identical in each experiment, and similar results were obtained when using a linear EOS or when removing seasonal variations of the forcing fields. This paper demonstrates the role of buoyancy forcing in setting the ocean’s large-scale stratification and the region of intermediate water formation.

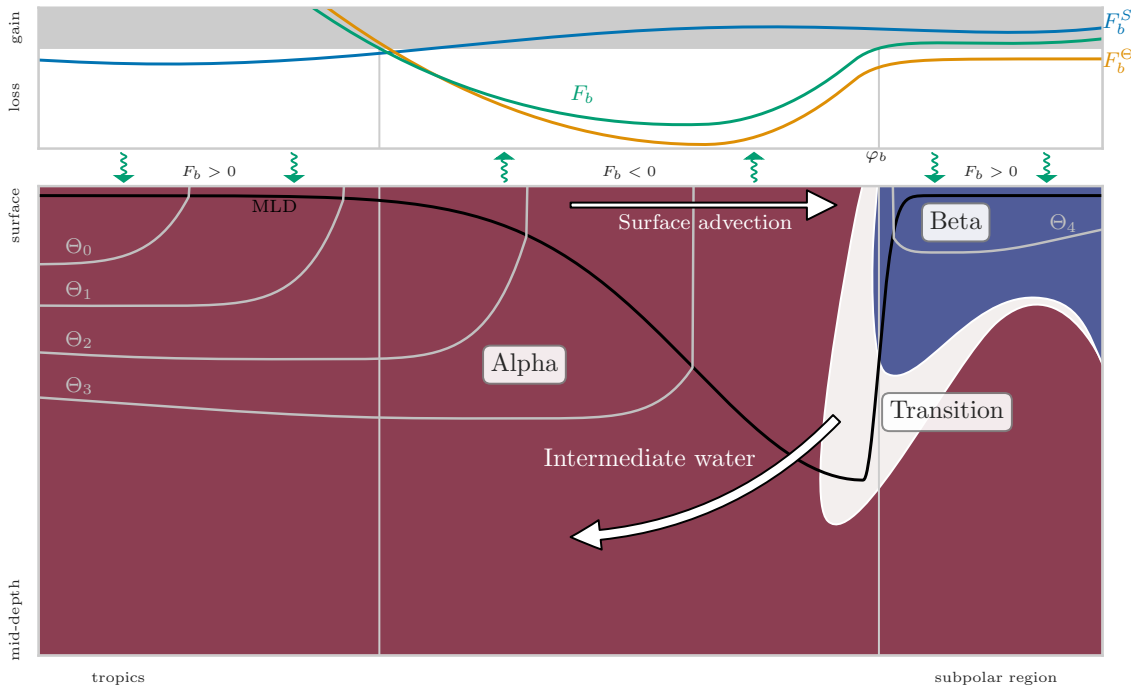


Figure 3.2: Conceptual view of the ocean. The upper panel represents annual buoyancy fluxes (F_b , green line) and its thermal (F_b^Θ , orange line) and haline (F_b^S , blue line) components. The green wavy arrows go upward when the ocean is losing buoyancy and they go upward when it is gaining it. In the bottom panel, the black line represents the mixed layer depth, red colours are for alpha ocean, white colours for transition zone, and blue colours for beta ocean. Figure from Caneill et al. (2022)

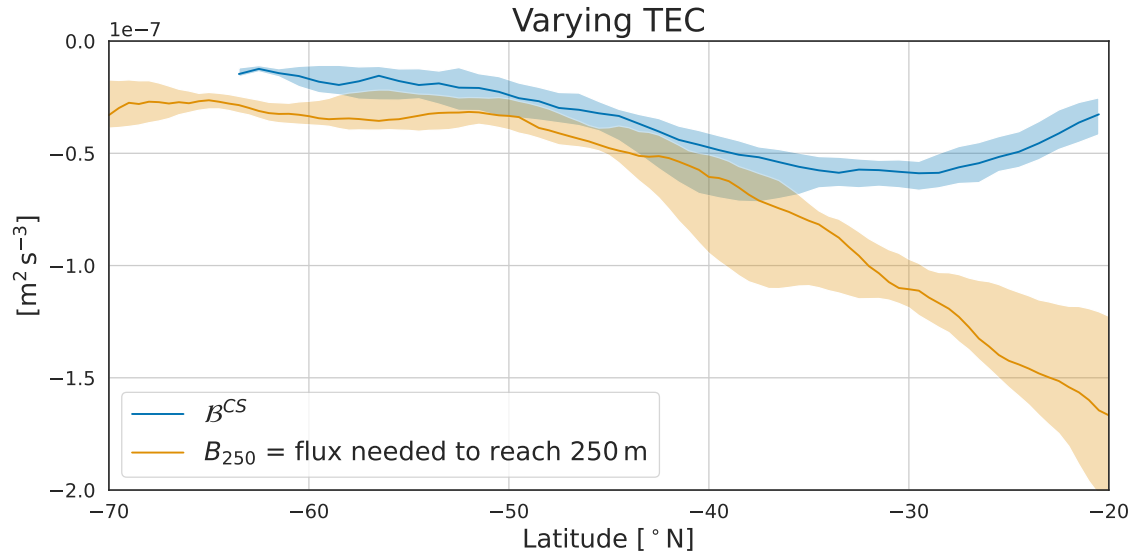


Figure 3.3: Buoyancy loss during the cooling season (B^{CS} , blue line) and stratification strength (B_{250} , orange line). The lines are zonal medians and the shadings are the first and third quartiles. The deep mixing band can occur where the two shaded curves cross. Figure adapted from Caneill et al. (2023).

3.4 Balance between seasonal buoyancy loss and stratification sets the deep mixing band (Paper II)

Processes of the SO, e.g., the Antarctic Circumpolar Current (ACC), large eddy activity, and sea ice, are not represented in the idealised basin model used in **Paper I**. We thus asked whether the existence and position of the DMB present in the SO could still be directly linked to buoyancy fluxes. For this, we computed climatologies of buoyancy fluxes and stratification based on observations (Chapters 2.2 and 2.3). A good correlation is found between annual surface buoyancy fluxes and the position of the DMB (Fig. 3c of **Paper II**). When adding Ekman buoyancy fluxes (Fig. 3i of **Paper II**), the DMB is located in the region of continuous buoyancy loss. South of it, the ocean is either positive or alternating between positive and negative in a patchy way. However, annual buoyancy loss in a region does not necessarily imply deep MLs in this region.

To fully explain the position of the DMB, one needs to take both the cooling season (CS) buoyancy loss and the summer stratification into account. Indeed, all the CS buoyancy loss erodes the summer stratification to produce the ML deepening. We found that the DMB is not necessarily located in areas of maximum CS buoyancy loss nor at the minimums of stratification (Fig. 3.3 and Fig. 3.4a and b). However, the DMB is systematically located where the CS buoyancy loss exceeds the stratification quantified by B_{250} (Fig. 3.4c). It results in a narrow band where the buoyancy loss can overcome the stratification. North of the DMB, the stratification is too large, and south of it, despite a small stratification, the buoyancy loss is too small. As in **Paper I**, we show here that the buoyancy loss is small because of the decrease in the TEC (Chapter 4) and not a decrease in heat loss. In regions of large advection of tropical water, as e.g., in the Agulhas Current, highly stratified water is continuously advected. Despite large heat losses, this blocks the formation of deep MLs.

3.5 Summary

Based on idealised numerical simulations and observations, this chapter explores the strong influence that buoyancy fluxes exert on the upper ocean stratification, summarised here:

- The deep MLs are found in regions of annual buoyancy loss at mid-latitudes. Poleward of these regions, the buoyancy flux is positive, and the oceans are losing heat and gaining freshwater. This allows for the formation of the halocline constituent of the beta oceans.
- The wind is found to not be of primary importance in setting the different stratification regimes. Wind stress forces the large-scale gyre circulation, but buoyancy fluxes directly impact the density and the stratification.
- The buoyancy loss during the CS fights against the summer stratification to deepen the ML. It is the balance between these two processes that,

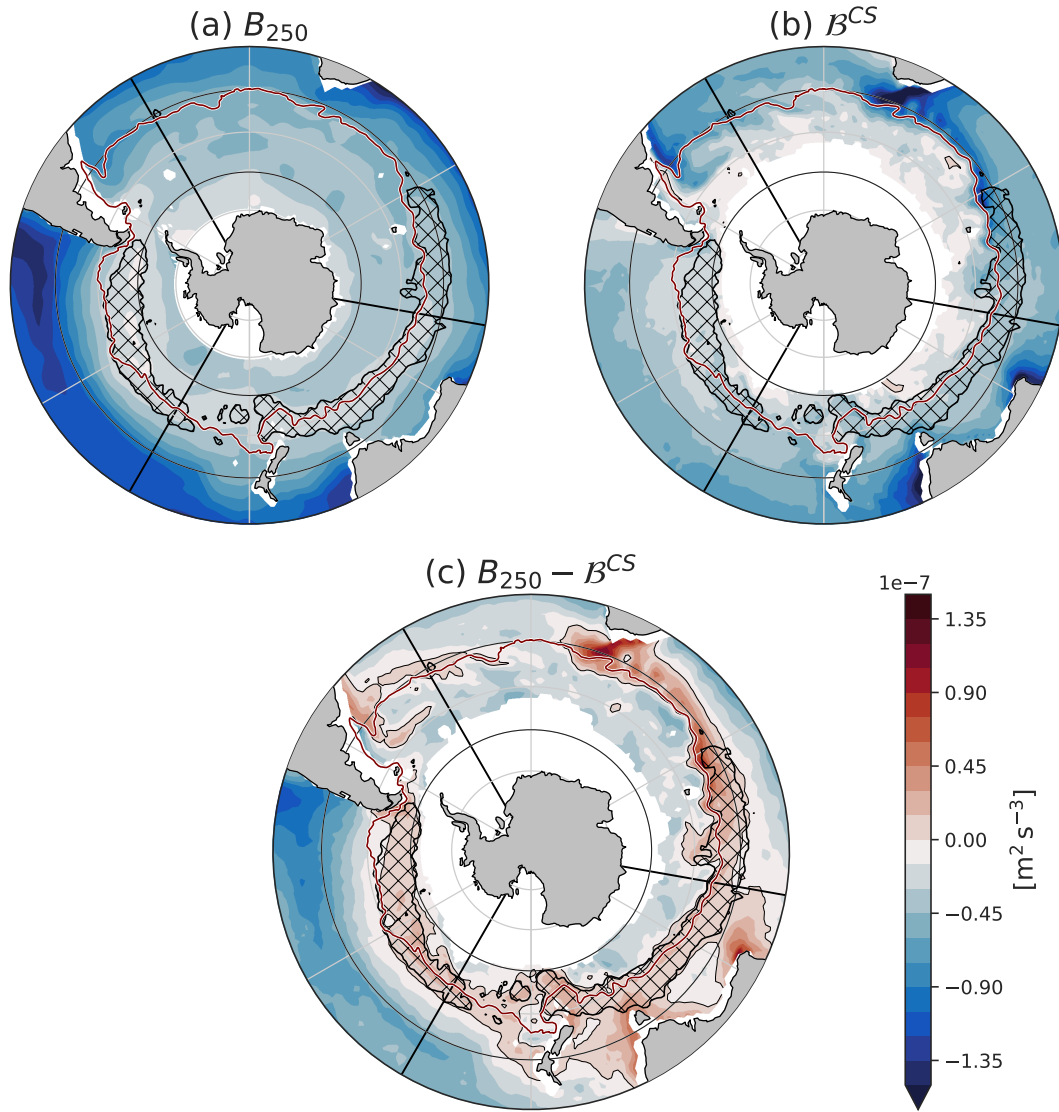


Figure 3.4: Climatology of (a) stratification strength, (b) buoyancy loss during the cooling season, and (c) the difference between them. The area hatched in black represent the observed deep mixing band. Figure adapted from Caneill et al. (2023).

eventually, sets the position of the deep MLs and ventilation regions. However, this balance is only valid away from regions where the western boundary currents advect highly stratified subtropical water and block the deepening of the ML.

- On the whole, buoyancy fluxes strongly constrain the possible regions of formation of deep MLs and, at the same time, control the upper ocean stratification regimes.

Chapter 4

The effects of the variable thermal expansion coefficient (Papers I, II, and IV)

4.1 Context

The thermal expansion coefficient (TEC), α , quantifies the relative change of density associated with a change of temperature:

$$\alpha(\Theta, S_A, p) = -\frac{1}{\rho} \left. \frac{\partial \rho}{\partial \Theta} \right|_{S_A, p} \quad (4.1)$$

where ρ is the water density, Θ the Conservative Temperature, S_A the Absolute Salinity, and p the pressure (Roquet et al., 2015a; IOC et al., 2015).

Freshwater temperature has the rare property that its density is maximal around 4°C at a pressure of 0 dbar. This implies that the TEC is negative below 4°C for freshwater (Fig. 4.1). A direct implication of this property is that dimictic lakes have a bottom temperature of 4°C all year long. However, the salinity of water in the oceans is greater than 30 g kg^{-1} , except in some small regions, e.g., the Baltic Sea. The effect of salinity on the TEC is to increase it, so in the oceans, the TEC is always positive (Fig. 4.1). Despite being positive, the TEC varies on the surface of the oceans, following an almost linear relationship with the sea surface temperature (SST), and is about ten times smaller at -2°C than at 30°C (Figs. 4.1 and 4.2). The variation of the TEC with temperature is the origin of the so-called cabbeling effect (described as “contraction under mixing”) (McDougall, 1987). The TEC is a function of pressure, which leads to an effect called thermobaricity. Isopycnal diffusion leads to diapycnal advection because of cabbeling and thermobaricity, which in turn impacts water mass transformation (Garrett & Horne, 1978; McDougall & You, 1990; Iudicone et al., 2008; Klocker & McDougall, 2010; Thomas & Shakespeare, 2015; Stewart & Haine, 2016; Groeskamp et al., 2016).

The temperature dependence of the TEC is not only a scientific curiosity, as it makes polar water density less sensitive to temperature changes than warm

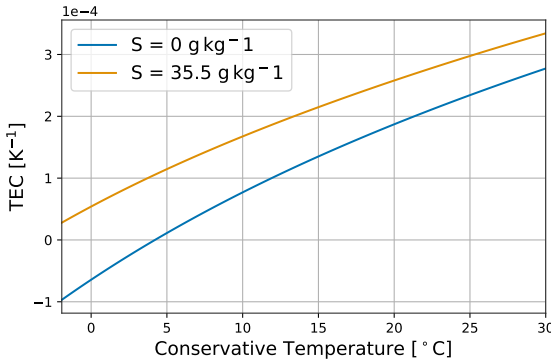


Figure 4.1: Thermal expansion coefficient function of Conservative Temperature at a pressure of 0 dbar. To highlight the role of salinity, two constant values for the Absolute Salinity are used: 0 g kg^{-1} (blue line) and 35.5 g kg^{-1} (orange line). Figure adapted from Caneill et al. (2023).

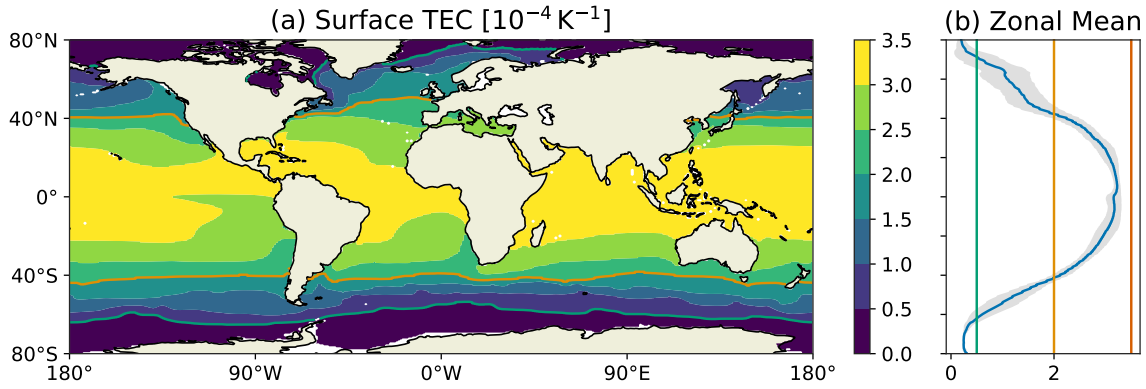


Figure 4.2: Map of the surface thermal expansion coefficient (a) and its zonal mean (b). The thermal expansion coefficient value is highly correlated with the sea surface temperature and shows almost an order of magnitude of variation in the oceans. The figures are based on ECCO. Figure adapted from Roquet et al. (2022).

water. As a result, salinity becomes more important in setting stratification in polar regions, and the importance of heat fluxes in buoyancy fluxes within polar regions is reduced (Rooth, 1982; Bryan, 1986; Aagaard & Carmack, 1989; Roquet et al., 2015b). Changes in the TEC value and variations impact the global circulation of the ocean (Roquet et al., 2015b; Nycander et al., 2015). The ocean gains heat in warm regions, and loses heat in cold regions, thus gaining more buoyancy (due to a large value of the TEC in warm water) than it loses (due to a small value of the TEC in cold water). With a balanced heat flux, this implies that the global buoyancy budget is positive (Garrett et al., 1993; Zahariev & Garrett, 1997; Hieronymus & Nycander, 2013). In a steady state, this positive budget of buoyancy fluxes thus balances the interior consumption of buoyancy by cabbeling. At a seasonal scale, variations of the TEC modulate the impact of summer and winter heat fluxes, so seasonal variations in the TEC increase the global buoyancy flux by 35% (Schanze & Schmitt, 2013).

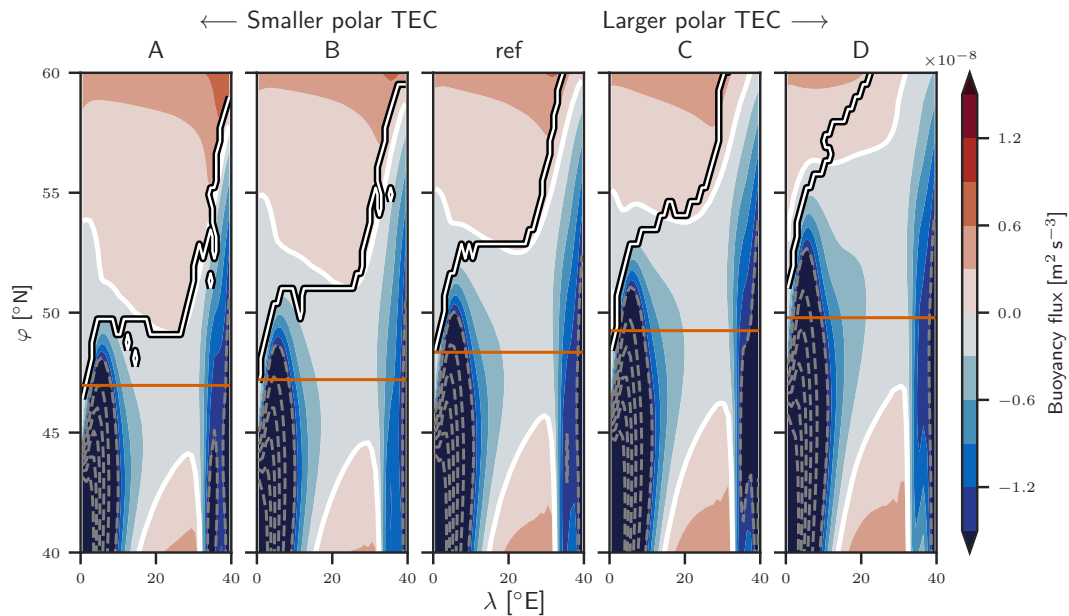


Figure 4.3: Annual buoyancy flux for every model run, ordered from lower to larger polar thermal expansion coefficient value. The white line with black contour represents the boundary between the alpha and beta oceans. Figure from Caneill et al. (2022).

4.2 The thermal expansion coefficient dampens the effect of heat fluxes in polar region (Papers I and II)

With the set of numerical experiments in **Paper I**, we were able to modify the value of the TEC in the subpolar region, thus subsequently changing the contribution of heat fluxes to buoyancy fluxes. As noted in earlier studies, the small polar value of the TEC is likely to weaken the contribution of heat fluxes (Rooth, 1982; Bryan, 1986; Aagaard & Carmack, 1989; Cerovečki et al., 2011), but this effect had not been intrinsically studied before. While keeping the same restoring conditions, an increased value of the TEC in the subpolar region of our basin led to a shrinking of the region of buoyancy loss towards the north. The buoyancy loss is driven by heat loss and counterbalanced by freshwater gain. When more importance is given to heat loss (through increased TEC), the polar area where buoyancy is gained decreases in size. This is what is observed in the basin runs (Fig. 4.3). When the buoyancy flux inversion gets pushed northward, the position of the polar transition zone (PTZ) follows.

In **Paper II**, based on heat flux products derived from observations, we computed the buoyancy fluxes of the cooling season (CS) in the SO, both with the varying TEC and with α_0 , a constant TEC representative of 40°S (Fig. 4.4a and b). Intense winter heat loss is driving the CS buoyancy loss in the Southern Ocean (SO). Taking the constant TEC increases the contribution of heat fluxes in the total buoyancy fluxes south of 40°S , where the surface water is colder than the reference value and hence the TEC is smaller. Opposite, north of 40°S , the constant TEC is smaller than what it should be, reducing the contribution of heat fluxes. The actual CS buoyancy loss using the varying TEC has a maximum intensity at 30°S and becomes abruptly close to zero south of it

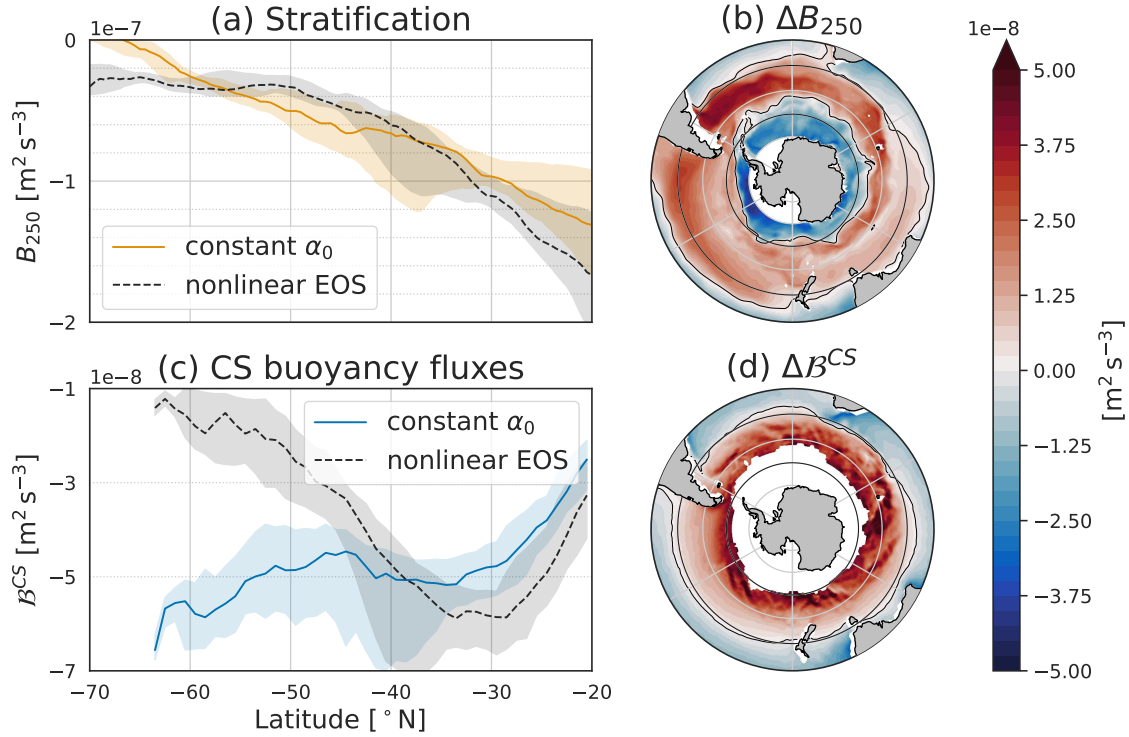


Figure 4.4: Stratification and buoyancy fluxes computed using either the varying thermal expansion coefficient or the constant α_0 . In panels (a) and (c), black dashed lines represent results with the varying thermal expansion coefficient, while blue or orange continuous lines represent results with the constant α_0 . The light shadings correspond to the 25th and 75th percentiles. Panels (b) and (d) are the differences between using the varying thermal expansion coefficient and the constant α_0 , for B_{250} and B^{CS} , respectively. Figure from Caneill et al. (2023).

(Fig. 4.4a, black dashed line). In contrast, when using the constant TEC, the buoyancy loss becomes increasingly important southwards, meaning that heat loss is not reduced southwards (Fig. 4.4a and b). The observed reduction of the winter buoyancy loss south of 40°S arises only because of the decrease in the TEC value and not because of a reduction in heat loss.

These two studies emphasise the substantial impact of the local value of the TEC in setting both annual and seasonal buoyancy fluxes.

4.3 The thermal expansion coefficient scales the effect of temperature on stratification (Papers I, II, and IV)

Paper I focuses on the role of buoyancy fluxes in setting the position of the transition zone. However, the effect of the TEC variations on the stratification is indirectly seen. Indeed, the northward migration of the PTZ (whose average latitude is called φ_β in the paper) is more significant than the one of the buoyancy flux inversion (whose latitude is called φ_b) when the polar vale of the TEC increases (evolution of φ_β and φ_b , Fig. 10 a and b of **Paper I**). This presumably comes from the fact that when the TEC increases in the beta ocean, stratifi-

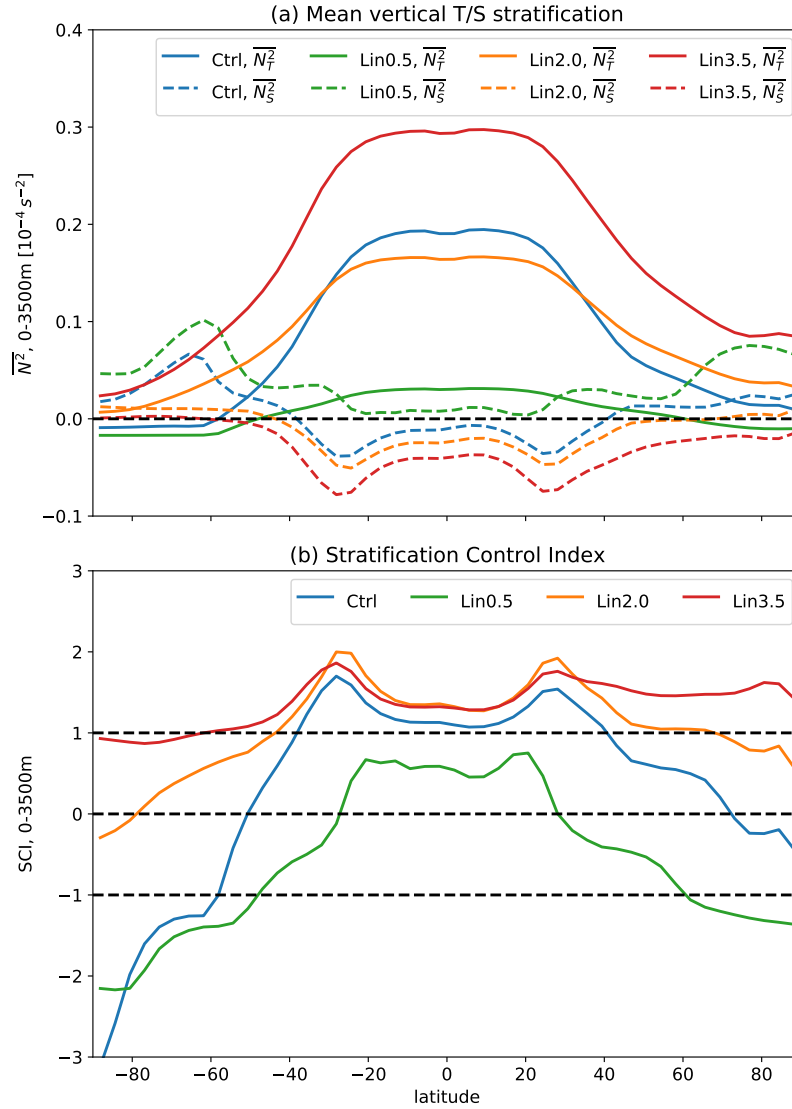


Figure 4.5: Zonal averages of (a) the temperature and salinity components of stratification and (b) the stratification control index for the aquaplanet model runs. The different colours represent different values of the thermal expansion coefficient used in these runs. Figure from Roquet et al. (2022).

cation decreases due to the temperature inversion. This effect alone shifts the PTZ northward. The effect of the buoyancy flux inversion is thus amplified.

In **Paper II**, using an observation-based climatology, we computed the stratification derived from the columnar buoyancy using either the local value of the TEC or the value representative of 40°S, α_0 . The difference between the two results corresponds to the effect of the variations of the TEC on stratification (Fig. 4.4c and d). North of 40°S, α_0 is smaller than the local value of the TEC, and the upper ocean is stratified by temperature. Thus, the stratification decreases when using α_0 . Between 40°S and 55°S, the local value of the TEC is smaller than α_0 while keeping a stratifying effect of temperature: using α_0 the constant TEC increases stratification. South of 55°S, the water column encounters a temperature inversion, and using α_0 enhances the destabilising effect of temperature, hence reducing stratification. We conclude that

a portion of the large subtropical stratification comes from the fact that the (varying) TEC is large. The decrease in stratification in the subpolar region is partly because of the decrease in TEC. Finally, the very low values of the TEC in the polar beta ocean stop the decrease in stratification that the temperature inversion would cause with larger TEC values.

Paper IV uses an ocean – atmosphere coupled numerical model on an idealised global configuration (an aquaplanet with two ridges representing the continents). A reference run (*Ctrl*) uses the full equation of state (EOS) and thus a varying TEC. Six runs with constant TEC are implemented (*LinX* with X in 0.5, 1.0, 1.25, 1.5, and 3.5 in units of $10^{-4} \text{ }^{\circ}\text{C}^{-1}$ the constant TEC). The differences between the circulation for each run thus arise from the direct impact of the value of the TEC and the indirect feedback. One main result of this study is that if the TEC is too large in the polar regions, the heat loss induces a large buoyancy loss that itself creates convection. This convection in the polar regions makes it impossible for sea ice to form; as soon as water is cold enough to freeze, it convects. Another result is that the stratification at one place using the varying TEC (nonlinear EOS) resembles the stratification at the same place, obtained with a constant value of the TEC close to the local value of the varying TEC (Fig. 4.5). Thus, the stratification control index (SCI) of the whole water column with a constant low value of the TEC (*Lin0.5*, green curves, Fig. 4.5) is close to the SCI resulting from the nonlinear EOS (*Ctrl*, blue curves) in polar regions. In contrast, *Lin0.5* is the run that produces the largest difference in stratification in tropical regions, where the difference between the values of the TEC between *Ctrl* and *Lin0.5* is the largest. A similar effect applies for *Lin2.0* and *Lin3.5*: they represent well the tropical stratification, but very poorly the polar stratification, to the point that no beta ocean exists any more.

4.4 Combined effect of the thermal expansion coefficient: application to the deep mixing band (Paper II)

Taking the balance between buoyancy loss during the CS and stratification strength allows predicting the location and width of the deep mixing band (DMB) (Chapter 3.4). Using the same balance but α_0 the constant TEC in calculation, we determined the combined effect of the TEC on buoyancy fluxes and on stratification (**Paper II**). Where buoyancy fluxes are more negative than stratification measured by B_{250} , the mixed layer (ML) induced by buoyancy loss reaches 250 m or goes deeper. The DMB is present between 35°S and 50°S, but contrary to reality in this case, it even extends to Antarctica (Fig. 4.6). South of 50°S, the mixed layer depths (MLDs) are deeper than 250 m. With a constant TEC, the DMB would not be a “band” any more but would maybe be called “deep mixing Southern Ocean”. A constant TEC would produce deep MLs everywhere in the SO, but in reality, they are only observed in the narrow DMB. This is thus the decrease of the TEC at low temperatures that sets the southern extent of the DMB. In reality, the low value of the TEC south of the DMB induces a reduction in buoyancy loss during the CS. This small buoyancy

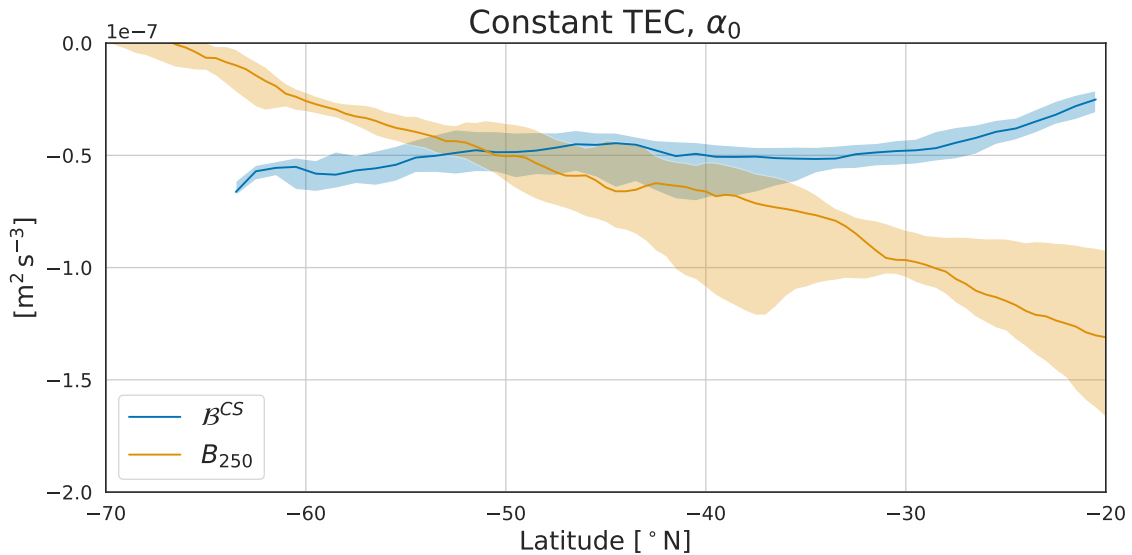


Figure 4.6: Buoyancy loss during the CS (\mathcal{B}^{CS} , blue line) and stratification strength (B_{250} , orange line), using the constant thermal expansion coefficient, α_0 , for the calculations. The lines are zonal medians and the shadings are the first and third quartiles. The DMD could occur where \mathcal{B}^{CS} becomes more negative than B_{250} . Figure adapted from Caneill et al. (2023).

loss is not able to destroy the stratification and produce deep MLs, despite a decrease in the stratification strength induced by the low values of the TEC.

4.5 Can we distinguish the effect of the thermal expansion coefficient on buoyancy fluxes and on stratification?

The effects of the TEC on upper ocean stratification and on buoyancy fluxes are not easily distinguishable, particularly in model runs where both effects are linked. When the ocean loses (gains) heat, its upper density increases (decreases) more or less depending on the value of the TEC. The buoyancy fluxes quantify this change. If the water column were to uniformly gain heat at every depth, the vertical temperature gradient would stay constant. However, due to the change in temperature, the TEC would change, changing the stratification strength at the same time. There are thus two distinguished roles of the TEC: one in scaling heat fluxes and the other in scaling temperature stratification.

In parts of the ocean, these two effects partly compensate for each other, slightly decreasing the importance of the value of the TEC in these regions. This is, for example, what happens in the subtropic (subpolar region), where using a smaller (larger) value of the TEC decreases (increases) stratification but also decreases (increases) the buoyancy loss during the CS (Figs. 4.4a and 4.4c north of 55°S). In the polar beta oceans, however, as they are regions of winter heat loss where temperature has a destabilising effect, an increase in the TEC value increases the buoyancy loss while decreasing the stratification. Beta oceans are thus regions where the value of the TEC is of primary importance in controlling the upper stratification.

4.6 Summary of the effects of the thermal expansion coefficient variations on global scale

The three papers described in this chapter provide an overview of the effect of TEC values on a global scale. I conclude this chapter by summarising these effects:

- Large TEC values in the subtropics are producing a large upper ocean stratification. This effect is damped by the fact that the large value of the TEC also enhances the winter buoyancy loss induced by heat fluxes.
- In the subantarctic zone (between 55°S and 40°S), the TEC has a relatively small value, which decreases the stratification (induced by temperature). At the same time, this small value damps the effect of heat fluxes on buoyancy fluxes. The effect of the damping of heat fluxes is to limit the southward extent of the DMB.
- In the beta ocean, the TEC is the smallest, thus making the temperature inversion possible. It also makes heat fluxes very inefficient at changing density. This is the region where the role of the TEC is most important. Opposite to the subtropics and subantarctic zone, the effect of the small value of the TEC is to increase stratification, both directly by reducing the impact of the temperature inversion on stratification and indirectly by making the winter buoyancy loss very small.
- Overall, it is the fact that the TEC becomes small in cold water that allows the formation of beta oceans. The halocline present in beta oceans limits the deepening of the MLs and allows for sea-ice formation.

Chapter 5

Characterising alpha and beta oceans from observations (Paper III)

5.1 Context

Previous studies have discussed a relation between ocean stratification and the horizontal zonation of the ocean. In the Southern Ocean (SO), Pollard et al. (2002) proposed to relate the Subantarctic Front (SAF) and Polar Front (PF) to boundaries between different regimes of thermohaline stratification. Carmack (2007) proposed the terms “alpha” and “beta” oceans to distinguish the effects of temperature and salinity on stratification. These two studies were, however, only based on a few hydrographic transects. On a global scale, You (2002), Helber et al. (2012), Stewart and Haine (2016), and Clément et al. (2020) produced maps to quantify the role of temperature and salinity in setting the stratification. Here we aim at mapping more accurately the different regimes and revealing an underlying relationship with the MLD distribution. As we focus on the stratification control index (SCI) below the mixed layer (ML), our approach is slightly different from the cited studies. Moreover, we use the EN4 database of temperature and salinity profiles from 2004 to 2021 to produce our mixed layer depth (MLD) and SCI climatologies, which extends the time period compared to previous studies. Further, computing the SCI directly on the profiles increases the accuracy of the results.

5.2 Climatologies of the stratification control index

In winter, the tropical regions around the equator have a SCI between -1 and 1 and are thus classified as transition zones (Figs. 5.1 and 5.2). They are regions gaining heat at the surface and, at the same time, gaining a substantial amount of freshwater through rain. These two fluxes are creating a warm, fresh, and highly stratified layer with a MLD around 50 m. Poleward of the tropical regions are found alpha oceans, with a winter $SCI > 1$. The MLD

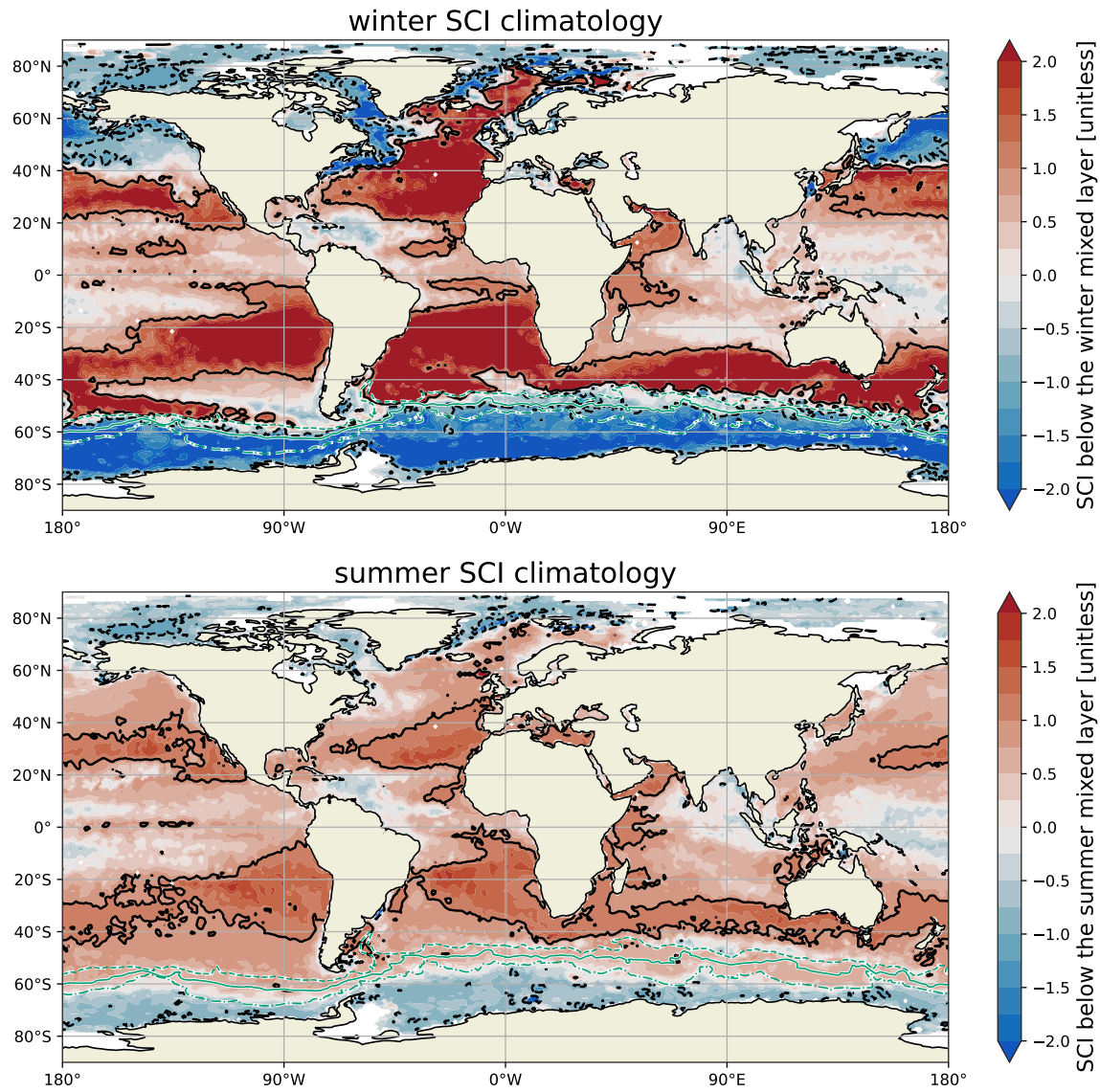


Figure 5.1: Stratification control index below the winter mixed layer (upper panel) and below the summer mixed layer (lower panel). The colours are saturated at $SCI = \pm 2$. The ocean is red where temperature predominantly stratifies, and blue where salinity predominantly stratifies. The continuous (dashed) black lines mark $SCI = 1$ ($SCI = -1$). Figure adapted from Caneill and Roquet (2023).

varies in these alpha oceans, from less than 100 m on the equator side to more than 300 m in the SO deep mixing band (DMB) and in the North Atlantic (**Paper III**). In the North Atlantic, there is a large interannual variability; for example, in the Irminger Sea, where deep convection occurs, MLDs of 400 m in 2014 were followed the next year by MLDs of 1200 m. Interannual variability is also found in the DMB but is less extreme.

A narrow polar transition zone (PTZ) is present in the SO and North Atlantic basin between the alpha and beta oceans, below the winter ML. In the North Pacific Ocean, the PTZ is only narrow on the western side and gets wider towards the east, becoming 20 degrees wide in latitude. In the South Pacific Ocean, a tongue of transition zone also exists. A main difference be-

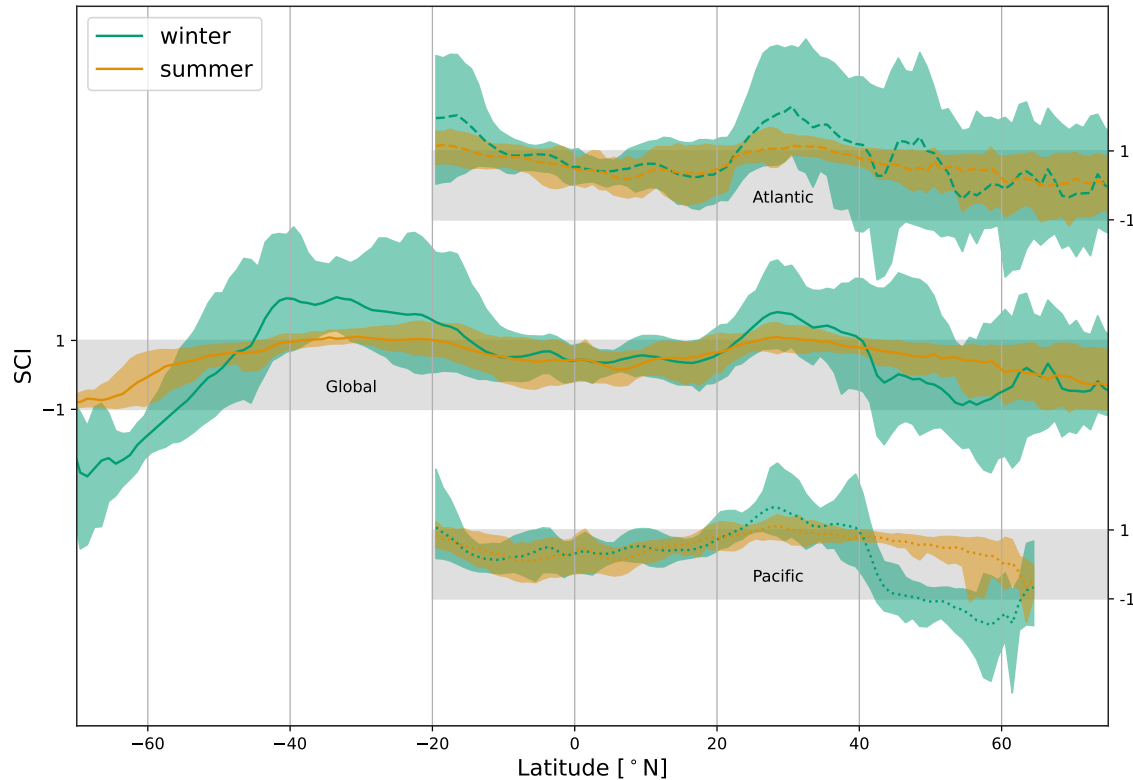


Figure 5.2: Zonal climatology of winter (green) and summer (orange) stratification control index below the mixed layer. The lines are the zonal means, and the shadings are the 10th and 90th percentiles. The middle lines are the global zonal means. The upper and lower lines, starting at 20°S, separate the Pacific basin, where the stratification control index is approximately zonally constant, from the Atlantic basin, where the stratification control index encounters large longitudinal variations. The Atlantic and Pacific zonal means have been shifted vertically for clarity, and they refer to their own axis on the right. The gray bands represent $-1 < SCI < 1$. Figure adapted from Caneill and Roquet (2023).

tween the South and North Pacific transition zones is that the south tongue is surrounded by alpha ocean before merging with the PTZ west of Drake Passage. In the North Pacific Ocean, the separation between the alpha and beta oceans follows an almost east-west direction. On the other hand, in the North Atlantic basin, the alpha ocean stretches northward along the European coast, while the beta ocean extends southward along the eastern coast of Greenland and the American coast. The separation thus follows a north-east diagonal.

The summer picture looks quite different (Fig. 5.1, lower panel, and Fig. 5.2). The SCI is generally smaller (in absolute value) during the summer than in the winter. It is larger than -1 everywhere and exceeds 1 only in parts of the subtropical regions. The SCI of the PTZ in the North Pacific basin shifts from a negative value in winter to a positive value in summer (visible between 40°N and 60°N, Fig. 5.2) and is almost the only region where the SCI changes sign between winter and summer. The main tendency is that the SCI value gets damped during the summer while keeping its sign.

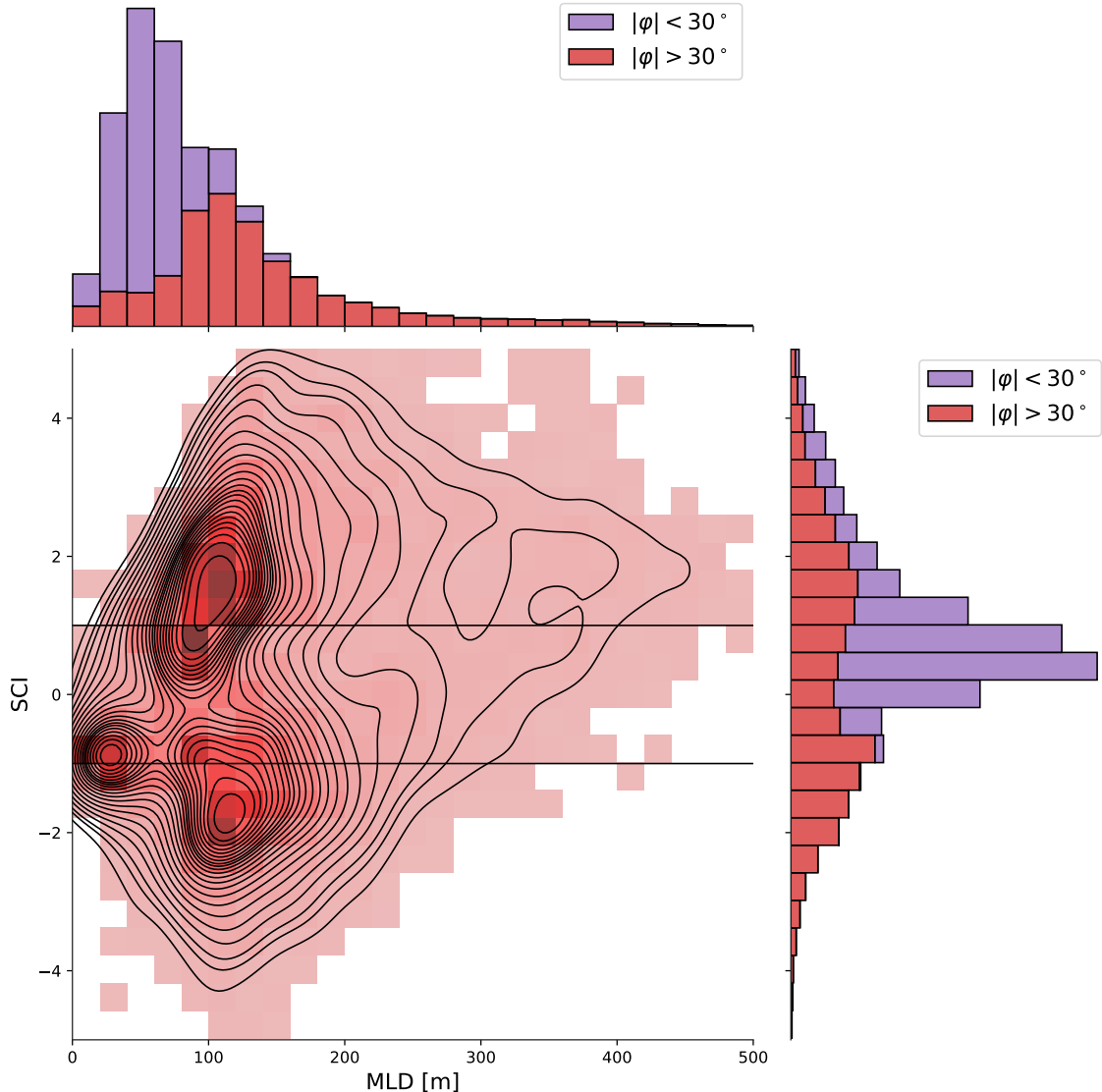


Figure 5.3: Stratification control index versus mixed layer depth in winter. The centre figure represents a 2 dimensions histogram (colours), with a kernel density estimation (contour lines) superimposed. For the centre figure, only data with a latitude $|\varphi| > 30^\circ$ are shown. The histograms on the sides are split into the tropical regions ($|\varphi| < 30^\circ$) in purple, and the rest of the ocean ($|\varphi| > 30^\circ$) in red. The upper histogram is for the mixed layer depth, and the histogram on the right is for the stratification control index. Data are taken from the winter 1° climatology. Each data point is weighted by the area of its corresponding cell of the 1° grid. Figure adapted from Caneill and Roquet (2023).

5.3 On the link with the mixed layer depth

Deep MLs seem to occur more often in alpha oceans than in beta oceans or transition zones (**Paper III**, compare maps of the MLD and the SCI, Figs. 3 and 7). This impression is confirmed when plotting the SCI versus the MLD (Fig. 5.3). MLs deeper than 250 m are mostly found in the alpha oceans (larger values of the two-dimensional histogram, Fig. 5.3). Deep MLs are also found in oceans classified as transition zones and are almost absent in beta oceans. Indi-

vidual profiles in the beta oceans show deep MLs along the coast of Antarctica, but they represent a small area and are thus not seen in this figure.

Tropical regions (defined here with an absolute value of the latitude less than 30°) are only plotted on the top and right histograms. They represent a large area with shallow MLs (less than 100 m) and are classified almost exclusively as transition zones.

For higher latitudes ($|\varphi| \geq 30^\circ$), the ML distribution exhibits a peak at 120 m. The SCI distribution poleward of 30° is bimodal, centred around ± 1.5 . The oceans thus encounter partial compensation between temperature and salinity more often than when temperature and salinity both stabilise. Poleward of 30° , the shallowest MLs are found in regions where salinity dominates the stratification ($SCI < 0$), either in transition zones or beta oceans. Regions that encounter large density compensation (large $|SCI|$) do not present shallow ML.

5.4 Summary

This chapter provides new insights on the zonation of the oceans between the alpha, transition, and beta regimes, and its propensity to encounter density compensation between temperature and salinity. To sum up, here is a summary:

- We confirm the zonation of alpha oceans at mid-latitudes, beta oceans at high latitudes, and the PTZs in between. However, **Paper III** reveals large differences in the structure between the North Atlantic and North Pacific basins. The North Pacific PTZ is almost zonal and becomes very wide eastward. Opposite, the North Atlantic PTZ is very narrow and follows a diagonal into the northwest.
- Except for the tropical oceans, the distribution of the SCI is bimodal, with the modes centred around $SCI = \pm 1.5$. The ocean in general tends to go towards temperature and salinity compensation rather than being doubly stabilised.
- Both in the North Atlantic basin and in the SO, deep MLs occur in the alpha ocean, near the boundary with the PTZ.
- Overall, the climatology of the winter SCI provides a global view of the oceans, where the regimes of stratification are highlighted. This allows for a precise determination of the role of temperature and salinity in setting the stratification.

Chapter 6

Conclusions and Outlook

In this thesis, we examined the mechanisms governing the zonation of the upper ocean stratification into different regimes, and specifically: Why and where is there a shift from alpha to beta oceans? For this, we studied the link between buoyancy fluxes and stratification. Using an idealised basin-like numerical model in **Paper I**, we found that the transition was located close to the sign inversion of the annual buoyancy fluxes. Buoyancy gain driven by positive freshwater fluxes in the northernmost part of the basin was creating a strong halocline, which was acting as a strong freshwater cap, preventing convection from occurring there. In **Paper II**, we used observational data to compare the autumn – winter buoyancy loss with the stratification strength of the upper ocean at the end of summer. We found that the simple balance between them is sufficient to explain the formation and shape of the DMB. Close to the strong western boundary currents (e.g., the Agulhas Current or the East Australian Current), highly stratified water is advected and the balance does not hold any more, thus no deep ML is formed despite strong buoyancy loss in winter. South of the DMB, the drop in the value of the TEC makes winter heat loss inefficient to increase density, limiting the southern extent of the DMB.

The type of stratification, quantified by the stratification control index (SCI), is linked to the position of the Subantarctic Front (SAF) and Polar Front (PF) in the Southern Ocean (SO) (**Paper III**). Defining circumpolar fronts using the SCI may not be very practical, as the SAF is surrounded by winter transition zones in the southeast Pacific Ocean while being at the boundary between the alpha ocean and transition zone elsewhere. However, a broad consistency is revealed, as well as large structural disparities around the SO. In summer, the entire SO is stratified by temperature below the mixed layer (ML) ($SCI \geq -1$), south of the Southern Boundary (SB) front, $SCI \geq 0$ which means that salinity is the dominant stratifying agent. The SB, defined with a dynamic definition, thus matches a stratification front. The stratification front may partly arise from the path of the water masses and advection. Globally, the absolute value of the SCI is larger in winter than in summer. This indicates that large density compensations occur between temperature and salinity

below the winter ML. Moreover, the summer SCI is between -1 and 1 everywhere, meaning that both temperature and salinity increase stratification below the summer ML. One exception is in the centre of the subtropical gyres, where $SCI > 1$.

Deep winter MLs are found in the alpha oceans, mainly in the deep mixing band (DMB) and in the Nordic Seas. In these regions, winter heat loss is the key component of convection. Opposite, close to the Antarctic coast, the surface temperature is at freezing point, so water cannot cool more to change density. Moreover, the value of the thermal expansion coefficient (TEC) makes any temperature change negligible for stratification. However, winter heat loss makes seawater freeze, increasing salinity through brine rejection and leading to convection. The driver of convection is thus different in alpha and beta oceans.

One key hypothesis of this thesis was that the origin of the transition between alpha and beta lies in the equation of state (EOS) and, more specifically, in the fact that the local value of the TEC is not the same everywhere on Earth. Artificially increasing the value of the TEC in the subpolar region leads to a decrease in the area of the beta ocean (**Paper I**). Further, it also increased the winter buoyancy loss, thus pushing the convective zone poleward and reducing the area available for the beta ocean. The local value of the TEC also scales the effect of temperature on stratification. Thus, a large value of the TEC in the polar regions makes it impossible to maintain a temperature inversion (**Paper IV**), making it impossible for sea ice to form. In **Paper II**, we found that the low value of the TEC south of the SAF damps a lot the winter heat loss effect on buoyancy, and despite a small stratification, no deep ML is formed. The decrease in the TEC is thus the origin of the southern boundary of the DMB. In both **Paper I** and **Paper IV**, we concluded that the cabbeling effect (defined as “contraction under mixing”) is not necessary to explain the alpha – beta transition in the ocean. On the contrary, it is the *local* value of the TEC that sets the stratification.

The work conducted in this thesis contributes to the understanding of the role of the intrinsic properties of seawater in large-scale circulation. We showed that the local value of the TEC scales both the effect of temperature on stratification, and of heat fluxes on buoyancy. This scaling is obvious when looking at the equations, but the effect of this scaling on the global circulation and stratification of the ocean remained to be investigated. To the question “Why is there a shift from alpha to beta oceans?” my answer is: “The shift occurs because at high latitudes the formation of beta oceans is forced by the small value of the TEC in cold water”. The zonation between the different regimes is mainly a consequence of the surface buoyancy fluxes over the oceans.

This thesis answers some questions but, at the same time, opens new horizons. Here are some future perspectives that I would like to see investigated in the future:

- Computing the SCI at the bottom of the ML is an efficient way to produce a global view of the upper ocean stratification. It can thus be used to compare and validate the different simulations that form the Coupled

Model Intercomparison Project (CMIP). The ocean is warming, so we can hypothesise that temperature will increase its control of the stratification, though the increase in the TEC. An increase in the TEC could also increase the buoyancy loss during winter. Deep MLs would shift poleward, and the surface of the beta oceans would decrease at the same time. Precise inspection of the CMIP outputs is necessary to verify the validity of these hypotheses.

- We concluded that cabbeling is not necessary to produce the polar transition zone (PTZ) between the alpha and beta oceans, but it would be useful to find a way to quantify its effect. There is, however, no easy way to do it because, as long as one uses a nonlinear EOS, the local values of the TEC will largely control the circulation. A possible way to have a varying TEC but no cabbeling would be to first run numerical simulations with the full EOS and to compute the buoyancy sink due to cabbeling. Then one could rerun the model with an extra term of buoyancy that would counterbalance the sink. This method would probably require a lot of changes in the model code, and closing the energy budget would probably be quite hard.
- Going beyond idealised simulation is an extra step that I would be happy to see achieved in the future. de Boer et al. (2007), Roquet et al. (2015b), and Nycander et al. (2015) have, for example, seen that the global circulation is sensitive to the EOS in realistic ocean simulations. Adding a fully coupled atmosphere could permit to gain more knowledge on the role of the TEC.
- By subducting heat and carbon, deep and intermediate waters mitigate the warming of the atmosphere. The DMB and the Nordic Seas convection are located in the alpha ocean, at the boundary of the transition zone. In a warming ocean, the value of the TEC increases, as does the role of temperature, both in stratification and buoyancy fluxes, directly impacting stratification. Changes in the stratification of these regions may directly impact the global climate. Global atmosphere – ocean coupled numerical simulations could be used to quantify the shift in the position of the transition zones and the feedback on the climate system.
- As water gets advected in the ML, it can encounter variations in the surface buoyancy flux due to the spatial variability of heat and freshwater fluxes. Following the water column from a Lagrangian perspective would tackle the issue that regions with large advection are forecasting deep MLs in **Paper II**, but they are not observed. Indeed, the Eulerian simple model of **Paper II** does not take the advection of stratified water into account. It would be possible to include this advection as an extra term in the model or compute the buoyancy fluxes along the trajectory using the Lagrangian frame. While not critical for the results of **Paper II**, using one of these two solutions would allow us to refine the analyses and study the interannual variability of the DMB, for example.

The climate would be very different if water had different physical and chemical properties. It is the remarkably large heat capacity and large latent heat of water that makes the ocean a very efficient heat conveyor. Among the specificities of the chemistry of water, we have focused in this thesis on the unique way the TEC varies with temperature. Owing to the large TEC values, the temperature easily stratifies the warm *alpha oceans*. However, at low temperatures, the TEC drops to near-zero values, letting salinity take control of the stratification and forming the cold *beta oceans*. It is interesting to notice that the observed heat and freshwater fluxes lead to comparable *surface buoyancy fluxes*. A uniform *seawater thermal expansion* coefficient would disrupt this delicate balance; temperature's effect would be too large or too small. Only the unique variations in the TEC allow both temperature and salinity to shape the *upper ocean stratification* in the way it is observed. The limited number of points of contact between the interior of the ocean and the atmosphere and the scarcity of vertical exchanges in the ocean generate the memory of the climate. Long-term climate change is therefore regulated by ocean breathing, which itself results from the subtle interplay between the thermodynamics of seawater and interactions with the atmosphere.

« En outre, j'ai surpris ces courants de haut en bas et de bas en haut, qui forment la vraie respiration de l'Océan. »
« *What's more, I've detected those falling and rising currents that make up the ocean's true breathing.* »

Capitaine Nemo, *Vingt mille lieues sous les mers*
Jules Verne, 1870

Bibliography

- Aagaard, K., & Carmack, E. C. (1989). The role of sea ice and other fresh water in the Arctic circulation. *Journal of Geophysical Research*, 94(C10), 14485. <https://doi.org/10.1029/JC094iC10p14485>
- Adler, R., Sapiano, M., Huffman, G., Wang, J.-J., Gu, G., Bolvin, D., Chiu, L., Schneider, U., Becker, A., Nelkin, E., Xie, P., Ferraro, R., & Shin, D.-B. (2018). The Global Precipitation Climatology Project (GPCP) Monthly Analysis (New Version 2.3) and a Review of 2017 Global Precipitation. *Atmosphere*, 9(4), 138. <https://doi.org/10.3390/atmos9040138>
- Årthun, M., Eldevik, T., Smedsrød, L. H., Skagseth, Ø., & Ingvaldsen, R. B. (2012). Quantifying the Influence of Atlantic Heat on Barents Sea Ice Variability and Retreat*. *Journal of Climate*, 25(13), 4736–4743. <https://doi.org/10.1175/JCLI-D-11-00466.1>
- Barkan, R., Winters, K. B., & Llewellyn Smith, S. G. (2013). Rotating horizontal convection. *Journal of Fluid Mechanics*, 723, 556–586. <https://doi.org/10.1017/jfm.2013.136>
- Barton, B. I., Lenn, Y.-D., & Lique, C. (2018). Observed Atlantification of the Barents Sea Causes the Polar Front to Limit the Expansion of Winter Sea Ice. *Journal of Physical Oceanography*, 48(8), 1849–1866. <https://doi.org/10.1175/JPO-D-18-0003.1>
- Belkin, I. M., & Gordon, A. L. (1996). Southern Ocean fronts from the Greenwich meridian to Tasmania. *Journal of Geophysical Research: Oceans*, 101(C2), 3675–3696. <https://doi.org/10.1029/95JC02750>
- Bindoff, N. L., & McDougall, T. J. (1994). Diagnosing Climate Change and Ocean Ventilation Using Hydrographic Data. *Journal of Physical Oceanography*, 24(6), 1137–1152. [https://doi.org/10.1175/1520-0485\(1994\)024<1137:DCCAOV>2.0.CO;2](https://doi.org/10.1175/1520-0485(1994)024<1137:DCCAOV>2.0.CO;2)
- Bryan, F. (1986). High-latitude salinity effects and interhemispheric thermohaline circulations. *Nature*, 323(6086), 301–304. <https://doi.org/10.1038/323301a0>
- Caneill, R., & Roquet, F. (2023). Temperature versus salinity: Distribution of stratification control in the global ocean. *in preparation for Ocean Science*.
- Caneill, R., Roquet, F., Madec, G., & Nycander, J. (2022). The Polar Transition from Alpha to Beta Regions Set by a Surface Buoyancy Flux Inversion. *Journal of Physical Oceanography*, 52(8), 1887–1902. <https://doi.org/10.1175/JPO-D-21-0295.1>
- Caneill, R., Roquet, F., & Nycander, J. (2023). Southern Ocean deep mixing band emerges from competition between winter buoyancy loss and stratification. *submitted to Ocean Science*. <https://doi.org/10.5194/egusphere-2023-2404>
- Carmack, E. C., Yamamoto-Kawai, M., Haine, T. W. N., Bacon, S., Bluhm, B. A., Lique, C., Melling, H., Polyakov, I. V., Straneo, F., Timmermans, M.-L., &

- Williams, W. J. (2016). Freshwater and its role in the Arctic Marine System: Sources, disposition, storage, export, and physical and biogeochemical consequences in the Arctic and global oceans. *Journal of Geophysical Research: Biogeosciences*, 121(3), 675–717. <https://doi.org/10.1002/2015JG003140>
- Carmack, E. C. (2007). The alpha/beta ocean distinction: A perspective on freshwater fluxes, convection, nutrients and productivity in high-latitude seas. *Deep Sea Research Part II: Topical Studies in Oceanography*, 54(23-26), 2578–2598. <https://doi.org/10.1016/j.dsr2.2007.08.018>
- CCHDO Hydrographic Data Office. (2023). CCHDO Hydrographic Data Archive, Version 2023-11-21 [In CCHDO Hydrographic Data Archive]. <https://doi.org/10.6075/J0CCHAM8>
- Cerovečki, I., Talley, L. D., & Mazloff, M. R. (2011). A Comparison of Southern Ocean Air–Sea Buoyancy Flux from an Ocean State Estimate with Five Other Products. *Journal of Climate*, 24(24), 6283–6306. <https://doi.org/10.1175/2011JCLI3858.1>
- Cess, R. D., & Goldenberg, S. D. (1981). The effect of ocean heat capacity upon global warming due to increasing atmospheric carbon dioxide. *Journal of Geophysical Research: Oceans*, 86(C1), 498–502. <https://doi.org/10.1029/JC086iC01p00498>
- Cessi, P. (2019). The Global Overturning Circulation. *Annual Review of Marine Science*, 11(1), 249–270. <https://doi.org/10.1146/annurev-marine-010318-095241>
- Clément, L., McDonagh, E. L., Marzocchi, A., & Nurser, A. J. G. (2020). Signature of Ocean Warming at the Mixed Layer Base. *Geophysical Research Letters*, 47(1). <https://doi.org/10.1029/2019GL086269>
- Cunningham, S. A., Alderson, S. G., King, B. A., & Brandon, M. A. (2003). Transport and variability of the Antarctic Circumpolar Current in Drake Passage. *Journal of Geophysical Research: Oceans*, 108(C5), 2001JC001147. <https://doi.org/10.1029/2001JC001147>
- Curry, J. A., Schramm, J. L., & Ebert, E. E. (1995). Sea Ice-Albedo Climate Feedback Mechanism. *Journal of Climate*, 8(2), 240–247. [https://doi.org/10.1175/1520-0442\(1995\)008<0240:SIACFM>2.0.CO;2](https://doi.org/10.1175/1520-0442(1995)008<0240:SIACFM>2.0.CO;2)
- de Boer, A. M., Sigman, D. M., Toggweiler, J. R., & Russell, J. L. (2007). Effect of global ocean temperature change on deep ocean ventilation. *Paleoceanography*, 22(2). <https://doi.org/10.1029/2005PA001242>
- de Boyer Montégut, C. (2004). Mixed layer depth over the global ocean: An examination of profile data and a profile-based climatology. *Journal of Geophysical Research*, 109(C12), C12003. <https://doi.org/10.1029/2004JC002378>
- de Boyer Montégut, C. (2023). Mixed layer depth climatology computed with a density threshold criterion of 0.03kg/m³ from 10 m depth value. <https://doi.org/10.17882/91774>
- de Verdière, C. A. (1988). Buoyancy driven planetary flows. *Journal of Marine Research*, 46(2), 215–265. <https://doi.org/10.1357/002224088785113667>
- Doney, S. C., Fabry, V. J., Feely, R. A., & Kleypas, J. A. (2009). Ocean Acidification: The Other CO₂ Problem. *Annual Review of Marine Science*, 1(1), 169–192. <https://doi.org/10.1146/annurev.marine.010908.163834>
- Dong, S., Sprintall, J., Gille, S. T., & Talley, L. (2008). Southern Ocean mixed-layer depth from Argo float profiles. *Journal of Geophysical Research*, 113(C6), C06013. <https://doi.org/10.1029/2006JC004051>

- DuVivier, A. K., Large, W. G., & Small, R. J. (2018). Argo Observations of the Deep Mixing Band in the Southern Ocean: A Salinity Modeling Challenge. *Journal of Geophysical Research: Oceans*, 123(10), 7599–7617. <https://doi.org/10.1029/2018JC014275>
- Emery, W. J. (1977). Antarctic Polar Frontal Zone from Australia to the Drake Passage. *Journal of Physical Oceanography*, 7(6), 811–822. [https://doi.org/10.1175/1520-0485\(1977\)007<0811:APFZFA>2.0.CO;2](https://doi.org/10.1175/1520-0485(1977)007<0811:APFZFA>2.0.CO;2)
- Faure, V., & Kawai, Y. (2015). Heat and salt budgets of the mixed layer around the Subarctic Front of the North Pacific Ocean. *Journal of Oceanography*, 71(5), 527–539. <https://doi.org/10.1007/s10872-015-0318-0>
- Forget, G., Campin, J.-M., Heimbach, P., Hill, C. N., Ponte, R. M., & Wunsch, C. (2015). Ecco version 4: An integrated framework for non-linear inverse modeling and global ocean state estimation. *Geoscientific Model Development*, 8(10), 3071–3104. <https://doi.org/10.5194/gmd-8-3071-2015>
- Garrett, C., Outerbridge, R., & Thompson, K. (1993). Interannual Variability in Mediterranean Heat and Buoyancy Fluxes. *Journal of Climate*, 6(5), 900–910. [https://doi.org/10.1175/1520-0442\(1993\)006<0900:IVIMHA>2.0.CO;2](https://doi.org/10.1175/1520-0442(1993)006<0900:IVIMHA>2.0.CO;2)
- Garrett, C., & Horne, E. (1978). Frontal circulation due to cabbeling and double diffusion. *Journal of Geophysical Research*, 83(C9), 4651. <https://doi.org/10.1029/JC083iC09p04651>
- Gill, A. E., & Adrian, E. (1982). *Atmosphere-ocean dynamics* (Vol. 30). Academic press.
- Good, S. A., Martin, M. J., & Rayner, N. A. (2013). EN4: Quality controlled ocean temperature and salinity profiles and monthly objective analyses with uncertainty estimates. *Journal of Geophysical Research: Oceans*, 118(12), 6704–6716. <https://doi.org/10.1002/2013JC009067>
- Gouretski, V., & Cheng, L. (2020). Correction for systematic errors in the global dataset of temperature profiles from mechanical bathythermographs. *Journal of Atmospheric and Oceanic Technology*, 37(5), 841–855.
- Gouretski, V., & Reseghetti, F. (2010). On depth and temperature biases in bathythermograph data: Development of a new correction scheme based on analysis of a global ocean database. *Deep Sea Research Part I: Oceanographic Research Papers*, 57(6), 812–833.
- Groeskamp, S., Abernathey, R. P., & Klocker, A. (2016). Water mass transformation by cabbeling and thermobaricity. *Geophysical Research Letters*, 43(20), 10, 835–10, 845. <https://doi.org/10.1002/2016GL070860>
- Gruber, N., Bakker, D. C. E., DeVries, T., Gregor, L., Hauck, J., Landschützer, P., McKinley, G. A., & Müller, J. D. (2023). Trends and variability in the ocean carbon sink. *Nature Reviews Earth & Environment*, 4(2), 119–134. <https://doi.org/10.1038/s43017-022-00381-x>
- Guinehut, S., Dhomps, A.-L., Larnicol, G., & Le Traon, P.-Y. (2012). High resolution 3-D temperature and salinity fields derived from in situ and satellite observations. *Ocean Science*, 8(5), 845–857. <https://doi.org/10.5194/os-8-845-2012>
- Hanawa, K., & Talley, L. D. (2001). Chapter 5.4 Mode waters [ISSN: 0074-6142]. In G. Siedler, J. Church, & J. Gould (Eds.), *Ocean Circulation and Climate* (pp. 373–386). Academic Press. [https://doi.org/https://doi.org/10.1016/S0074-6142\(01\)80129-7](https://doi.org/https://doi.org/10.1016/S0074-6142(01)80129-7)

- Helber, R. W., Kara, A. B., Richman, J. G., Carnes, M. R., Barron, C. N., Hurlburt, H. E., & Boyer, T. (2012). Temperature versus salinity gradients below the ocean mixed layer. *Journal of Geophysical Research: Oceans*, 117(C5), n/a–n/a. <https://doi.org/10.1029/2011JC007382>
- Herrmann, M., Somot, S., Sevault, F., Estournel, C., & Déqué, M. (2008). Modeling the deep convection in the northwestern Mediterranean Sea using an eddy-permitting and an eddy-resolving model: Case study of winter 1986–1987. *Journal of Geophysical Research*, 113(C4), C04011. <https://doi.org/10.1029/2006JC003991>
- Hieronymus, M., & Nylander, J. (2013). The Buoyancy Budget with a Nonlinear Equation of State. *Journal of Physical Oceanography*, 43(1), 176–186. <https://doi.org/10.1175/JPO-D-12-063.1>
- Holte, J. W., Talley, L. D., Chereskin, T. K., & Sloyan, B. M. (2012). The role of air-sea fluxes in Subantarctic Mode Water formation. *Journal of Geophysical Research: Oceans*, 117(C3). <https://doi.org/10.1029/2011JC007798>
- IOC, SCOR, & IAPSO. (2015). The International thermodynamic equation of seawater–2010: Calculation and use of thermodynamic properties.[includes corrections up to 31st October 2015]. *Intergovernmental Oceanographic Commission, Manuals and Guides*, 56, 220. http://teos-10.org/pubs/TEOS-10_Manual.pdf
- Isachsen, P. E., Mauritzen, C., & Svendsen, H. (2007). Dense water formation in the Nordic Seas diagnosed from sea surface buoyancy fluxes. *Deep Sea Research Part I: Oceanographic Research Papers*, 54(1), 22–41. <https://doi.org/10.1016/j.dsr.2006.09.008>
- Iudicone, D., Madec, G., Blanke, B., & Speich, S. (2008). The Role of Southern Ocean Surface Forcings and Mixing in the Global Conveyor. *Journal of Physical Oceanography*, 38(7), 1377–1400. <https://doi.org/10.1175/2008JPO3519.1>
- Johnson, G. C., Kunze, E., McTaggart, K. E., & Moore, D. W. (2002). Temporal and Spatial Structure of the Equatorial Deep Jets in the Pacific Ocean*. *Journal of Physical Oceanography*, 32(12), 3396–3407. [https://doi.org/10.1175/1520-0485\(2002\)032<3396:TASSOT>2.0.CO;2](https://doi.org/10.1175/1520-0485(2002)032<3396:TASSOT>2.0.CO;2)
- Karstensen, J., & Lorbacher, K. (2011). A practical indicator for surface ocean heat and freshwater buoyancy fluxes and its application to the NCEP reanalysis data. *Tellus A: Dynamic Meteorology and Oceanography*, 63(2), 338–347. <https://doi.org/10.1111/j.1600-0870.2011.00510.x>
- Klocker, A., Naveira Garabato, A. C., Roquet, F., De Lavergne, C., & Rintoul, S. R. (2023a). Generation of the Internal Pycnocline in the Subpolar Southern Ocean by Wintertime Sea Ice Melting. *Journal of Geophysical Research: Oceans*, 128(3), e2022JC019113. <https://doi.org/10.1029/2022JC019113>
- Klocker, A., & McDougall, T. J. (2010). Influence of the Nonlinear Equation of State on Global Estimates of Dianutral Advection and Diffusion. *Journal of Physical Oceanography*, 40(8), 1690–1709. <https://doi.org/10.1175/2010JPO4303.1>
- Klocker, A., Munday, D., Gayen, B., Roquet, F., & LaCasce, J. (2023b). Deep-reaching global ocean overturning circulation generated by surface buoyancy forcing [Accepted for publication]. *Tellus*.
- Kuhlbrodt, T., Griesel, A., Montoya, M., Levermann, A., Hofmann, M., & Rahmstorf, S. (2007). On the driving processes of the Atlantic meridional overturning circulation. *Reviews of Geophysics*, 45(2). <https://doi.org/10.1029/2004RG000166>

- Lambert, E., Eldevik, T., & Spall, M. A. (2018). On the Dynamics and Water Mass Transformation of a Boundary Current Connecting Alpha and Beta Oceans. *Journal of Physical Oceanography*, 48(10), 2457–2475. <https://doi.org/10.1175/JPO-D-17-0186.1>
- Lascaratos, A., & Nittis, K. (1998). A high-resolution three-dimensional numerical study of intermediate water formation in the Levantine Sea. *Journal of Geophysical Research: Oceans*, 103(C9), 18497–18511. <https://doi.org/10.1029/98JC01196>
- Lazier, J. R. (1980). Oceanographic conditions at Ocean Weather Ship Bravo, 1964–1974. *Atmosphere-Ocean*, 18(3), 227–238. <https://doi.org/10.1080/07055900.1980.9649089>
- Lévy, M., Klein, P., Tréguier, A.-M., Iovino, D., Madec, G., Masson, S., & Takahashi, K. (2010). Modifications of gyre circulation by sub-mesoscale physics. *Ocean Modelling*, 34(1-2), 1–15. <https://doi.org/10.1016/j.ocemod.2010.04.001>
- Madec, T., Gurvan and NEMO System. (2019). NEMO ocean engine. <https://doi.org/10.5281/ZENODO.1464816>
- Manabe, S., & Wetherald, R. T. (1967). Thermal Equilibrium of the Atmosphere with a Given Distribution of Relative Humidity. *Journal of the Atmospheric Sciences*, 24(3), 241–259. [https://doi.org/10.1175/1520-0469\(1967\)024<0241:TEOTAW>2.0.CO;2](https://doi.org/10.1175/1520-0469(1967)024<0241:TEOTAW>2.0.CO;2)
- Manabe, S., & Wetherald, R. T. (1975). The effects of doubling the co₂ concentration on the climate of a general circulation model. *Journal of Atmospheric Sciences*, 32(1), 3–15.
- Mauritzen, C., & Häkkinen, S. (1999). On the relationship between dense water formation and the “Meridional Overturning Cell” in the North Atlantic Ocean. *Deep Sea Research Part I: Oceanographic Research Papers*, 46(5), 877–894. [https://doi.org/10.1016/S0967-0637\(98\)00094-6](https://doi.org/10.1016/S0967-0637(98)00094-6)
- McDougall, T. J. (1987). Thermobaricity, cabbeling, and water-mass conversion. *Journal of Geophysical Research*, 92(C5), 5448. <https://doi.org/10.1029/JC092iC05p05448>
- McDougall, T. J., & You, Y. (1990). Implications of the nonlinear equation of state for upwelling in the ocean interior. *Journal of Geophysical Research*, 95(C8), 13263. <https://doi.org/10.1029/JC095iC08p13263>
- Meredith, M. (2019). The global importance of the southern ocean and the key role of its freshwater cycle. *Ocean Challenge*, 23.
- Munk, W. H. (1950). On the wind-driven ocean circulation. *Journal of Meteorology*, 7(2), 80–93. [https://doi.org/10.1175/1520-0469\(1950\)007<0080:OTWDOC>2.0.CO;2](https://doi.org/10.1175/1520-0469(1950)007<0080:OTWDOC>2.0.CO;2)
- Munk, W. H. (1966). Abyssal recipes. *Deep Sea Research and Oceanographic Abstracts*, 13(4), 707–730. [https://doi.org/10.1016/0011-7471\(66\)90602-4](https://doi.org/10.1016/0011-7471(66)90602-4)
- Naveira Garabato, A. C., Jullion, L., Stevens, D. P., Heywood, K. J., & King, B. A. (2009). Variability of Subantarctic Mode Water and Antarctic Intermediate Water in the Drake Passage during the Late-Twentieth and Early-Twenty-First Centuries. *Journal of Climate*, 22(13), 3661–3688. <https://doi.org/10.1175/2009JCLI2621.1>
- Nycander, J., Hieronymus, M., & Roquet, F. (2015). The nonlinear equation of state of sea water and the global water mass distribution: Global Water Mass Dis-

- tribution. *Geophysical Research Letters*, 42(18), 7714–7721. <https://doi.org/10.1002/2015GL065525>
- Oeschger, H., Siegenthaler, U., Schotterer, U., & Gugelmann, A. (1975). A box diffusion model to study the carbon dioxide exchange in nature. *Tellus*, 27(2), 168–192. <https://doi.org/10.1111/j.2153-3490.1975.tb01671.x>
- Onarheim, I. H., Eldevik, T., Årthun, M., Ingvaldsen, R. B., & Smedsrød, L. H. (2015). Skillful prediction of Barents Sea ice cover. *Geophysical Research Letters*, 42(13), 5364–5371. <https://doi.org/10.1002/2015GL064359>
- Park, Y.-H., Park, T., Kim, T.-W., Lee, S.-H., Hong, C.-S., Lee, J.-H., Rio, M.-H., Pujol, M.-I., Ballarotta, M., Durand, I., & Provost, C. (2019). Observations of the Antarctic Circumpolar Current Over the Udintsev Fracture Zone, the Narrowest Choke Point in the Southern Ocean. *Journal of Geophysical Research: Oceans*, 124(7), 4511–4528. <https://doi.org/10.1029/2019JC015024>
- Pauthenet, E., Roquet, F., Madec, G., & Nerini, D. (2017). A Linear Decomposition of the Southern Ocean Thermohaline Structure. *Journal of Physical Oceanography*, 47(1), 29–47. <https://doi.org/10.1175/JPO-D-16-0083.1>
- Pelichero, V., Sallée, J.-B., Chapman, C. C., & Downes, S. M. (2018). The southern ocean meridional overturning in the sea-ice sector is driven by freshwater fluxes. *Nature Communications*, 9(1), 1789. <https://doi.org/10.1038/s41467-018-04101-2>
- Perovich, D. K., & Polashenski, C. (2012). Albedo evolution of seasonal Arctic sea ice. *Geophysical Research Letters*, 39(8), 2012GL051432. <https://doi.org/10.1029/2012GL051432>
- Petit, T., Lozier, M. S., Josey, S. A., & Cunningham, S. A. (2020). Atlantic Deep Water Formation Occurs Primarily in the Iceland Basin and Irminger Sea by Local Buoyancy Forcing. *Geophysical Research Letters*, 47(22). <https://doi.org/10.1029/2020GL091028>
- Pollard, R., Lucas, M., & Read, J. (2002). Physical controls on biogeochemical zonation in the Southern Ocean. *Deep Sea Research Part II: Topical Studies in Oceanography*, 49(16), 3289–3305. [https://doi.org/10.1016/S0967-0645\(02\)00084-X](https://doi.org/10.1016/S0967-0645(02)00084-X)
- Polyakov, I. V., Pnyushkov, A. V., Rember, R., Padman, L., Carmack, E. C., & Jackson, J. M. (2013). Winter Convection Transports Atlantic Water Heat to the Surface Layer in the Eastern Arctic Ocean*. *Journal of Physical Oceanography*, 43(10), 2142–2155. <https://doi.org/10.1175/JPO-D-12-0169.1>
- Polzin, K. L., Toole, J. M., Ledwell, J. R., & Schmitt, R. W. (1997). Spatial Variability of Turbulent Mixing in the Abyssal Ocean. *Science*, 276(5309), 93–96. <https://doi.org/10.1126/science.276.5309.93>
- Rhines, P., Häkkinen, S., & Josey, S. A. (2008). Is Oceanic Heat Transport Significant in the Climate System? In R. R. Dickson, J. Meincke, & P. Rhines (Eds.), *Arctic–Subarctic Ocean Fluxes* (pp. 87–109). Springer Netherlands. https://doi.org/10.1007/978-1-4020-6774-7_5
- Ridge, S. M., & McKinley, G. A. (2021). Ocean carbon uptake under aggressive emission mitigation. *Biogeosciences*, 18(8), 2711–2725. <https://doi.org/10.5194/bg-18-2711-2021>
- Rintoul, S. R., & England, M. H. (2002). Ekman Transport Dominates Local Air–Sea Fluxes in Driving Variability of Subantarctic Mode Water. *Journal of Physical*

- Oceanography*, 32(5), 1308–1321. [https://doi.org/10.1175/1520-0485\(2002\)032<1308:ETDLAS>2.0.CO;2](https://doi.org/10.1175/1520-0485(2002)032<1308:ETDLAS>2.0.CO;2)
- Rooth, C. (1982). Hydrology and ocean circulation. *Progress in Oceanography*, 11(2), 131–149. [https://doi.org/10.1016/0079-6611\(82\)90006-4](https://doi.org/10.1016/0079-6611(82)90006-4)
- Roquet, F., Madec, G., McDougall, T. J., & Barker, P. M. (2015a). Accurate polynomial expressions for the density and specific volume of seawater using the TEOS-10 standard. *Ocean Modelling*, 90, 29–43. <https://doi.org/10.1016/j.ocemod.2015.04.002>
- Roquet, F., Ferreira, D., Caneill, R., Schlesinger, D., & Madec, G. (2022). Unique thermal expansion properties of water key to the formation of sea ice on Earth. *Science Advances*, 8(46). <https://doi.org/10.1126/sciadv.abq0793>
- Roquet, F., Madec, G., Brodeau, L., & Nycander, J. (2015b). Defining a Simplified Yet “Realistic” Equation of State for Seawater. *Journal of Physical Oceanography*, 45(10), 2564–2579. <https://doi.org/10.1175/JPO-D-15-0080.1>
- Rossow, W. B., & Schiffer, R. A. (1999). Advances in Understanding Clouds from ISCCP. *Bulletin of the American Meteorological Society*, 80(11), 2261–2287. [https://doi.org/10.1175/1520-0477\(1999\)080<2261:AIUCFI>2.0.CO;2](https://doi.org/10.1175/1520-0477(1999)080<2261:AIUCFI>2.0.CO;2)
- Ruddick, B. (1983). A practical indicator of the stability of the water column to double-diffusive activity. *Deep Sea Research Part A. Oceanographic Research Papers*, 30(10), 1105–1107. [https://doi.org/10.1016/0198-0149\(83\)90063-8](https://doi.org/10.1016/0198-0149(83)90063-8)
- Sabine, C. L., Feely, R. A., Gruber, N., Key, R. M., Lee, K., Bullister, J. L., Wanninkhof, R., Wong, C. S., Wallace, D. W. R., Tilbrook, B., Millero, F. J., Peng, T.-H., Kozyr, A., Ono, T., & Rios, A. F. (2004). The Oceanic Sink for Anthropogenic CO₂. *Science*, 305(5682), 367–371. <https://doi.org/10.1126/science.1097403>
- Sallée, J.-B., Speer, K., Rintoul, S., & Wijffels, S. (2010). Southern Ocean Thermocline Ventilation. *Journal of Physical Oceanography*, 40(3), 509–529. <https://doi.org/10.1175/2009JPO4291.1>
- Schanze, J. J., & Schmitt, R. W. (2013). Estimates of Cabbeling in the Global Ocean. *Journal of Physical Oceanography*, 43(4), 698–705. <https://doi.org/10.1175/JPO-D-12-0119.1>
- Schiffer, R. A., & Rossow, W. B. (1983). The international satellite cloud climatology project (isccp): The first project of the world climate research programme. *Bull. Amer. Meteorol. Soc.*, 64, 779–784.
- Schmidtko, S., Johnson, G. C., & Lyman, J. M. (2013). MIMOC: A global monthly isopycnal upper-ocean climatology with mixed layers: MIMOC. *Journal of Geophysical Research: Oceans*, 118(4), 1658–1672. <https://doi.org/10.1002/jgrc.20122>
- Schmitt, R. W. (1994). Double Diffusion in Oceanography. *Annual Review of Fluid Mechanics*, 26(1), 255–285. <https://doi.org/10.1146/annurev.fl.26.010194.001351>
- Schmitt, R. W., Bogden, P. S., & Dorman, C. E. (1989). Evaporation Minus Precipitation and Density Fluxes for the North Atlantic. *Journal of Physical Oceanography*, 19(9), 1208–1221. [https://doi.org/10.1175/1520-0485\(1989\)019<1208:EMPADF>2.0.CO;2](https://doi.org/10.1175/1520-0485(1989)019<1208:EMPADF>2.0.CO;2)
- Sloyan, B. M., & Rintoul, S. R. (2001). Circulation, Renewal, and Modification of Antarctic Mode and Intermediate Water. *Journal of Physical Oceanography*,

- 31(4), 1005–1030. [https://doi.org/10.1175/1520-0485\(2001\)031<1005:CRAMOA>2.0.CO;2](https://doi.org/10.1175/1520-0485(2001)031<1005:CRAMOA>2.0.CO;2)
- Sohail, T., Vreugdenhil, C. A., Gayen, B., & Hogg, A. M. (2019). The Impact of Turbulence and Convection on Transport in the Southern Ocean. *Journal of Geophysical Research: Oceans*, 124(6), 4208–4221. <https://doi.org/10.1029/2018JC014883>
- Speer, K., Isemer, H.-J., & Biastoch, A. (1995). Water Mass Formation from Revised COADS Data. *Journal of Physical Oceanography*, 25(10), 2444–2457. [https://doi.org/10.1175/1520-0485\(1995\)025<2444:WMFFRC>2.0.CO;2](https://doi.org/10.1175/1520-0485(1995)025<2444:WMFFRC>2.0.CO;2)
- Speer, K., Rintoul, S. R., & Sloyan, B. (2000). The Diabatic Deacon Cell. *Journal of Physical Oceanography*, 30(12), 3212–3222. [https://doi.org/10.1175/1520-0485\(2000\)030<3212:TDDC>2.0.CO;2](https://doi.org/10.1175/1520-0485(2000)030<3212:TDDC>2.0.CO;2)
- Sprintall, J., & Cronin, M. F. (2009). Upper Ocean Vertical Structure. In J. H. Steele (Ed.), *Encyclopedia of Ocean Sciences (Second Edition)* (Second Edition, pp. 217–224). Academic Press. <https://doi.org/https://doi.org/10.1016/B978-012374473-9.00627-5>
- Stern, M. E. (1960). The “Salt-Fountain” and Thermohaline Convection. *Tellus*, 12(2), 172–175. <https://doi.org/10.3402/tellusa.v12i2.9378>
- Stewart, K. D., & Haine, T. W. N. (2016). Thermobaricity in the Transition Zones between Alpha and Beta Oceans. *Journal of Physical Oceanography*, 46(6), 1805–1821. <https://doi.org/10.1175/JPO-D-16-0017.1>
- Stommel, H. (1948). The westward intensification of wind-driven ocean currents. *Eos, Transactions American Geophysical Union*, 29(2), 202–206.
- Stommel, H. (1958). The abyssal circulation. *Deep Sea Research (1953)*, 5(1), 80–82. [https://doi.org/10.1016/S0146-6291\(58\)80014-4](https://doi.org/10.1016/S0146-6291(58)80014-4)
- Stommel, H. (1961). Thermohaline Convection with Two Stable Regimes of Flow. *Tellus*, 13(2), 224–230. <https://doi.org/10.1111/j.2153-3490.1961.tb00079.x>
- Stommel, H., & Arons, A. (1959). On the abyssal circulation of the world ocean—I. Stationary planetary flow patterns on a sphere. *Deep Sea Research (1953)*, 6, 140–154. [https://doi.org/10.1016/0146-6313\(59\)90065-6](https://doi.org/10.1016/0146-6313(59)90065-6)
- Sverdrup, H. U. (1947). Wind-Driven Currents in a Baroclinic Ocean; with Application to the Equatorial Currents of the Eastern Pacific. *Proceedings of the National Academy of Sciences*, 33(11), 318–326. <https://doi.org/10.1073/pnas.33.11.318>
- Thomas, L. N., & Shakespeare, C. J. (2015). A New Mechanism for Mode Water Formation involving Cabbeling and Frontogenetic Strain at Thermohaline Fronts. *Journal of Physical Oceanography*, 45(9), 2444–2456. <https://doi.org/10.1175/JPO-D-15-0007.1>
- Toggweiler, J. R., & Samuels, B. (1998). On the Ocean’s Large-Scale Circulation near the Limit of No Vertical Mixing. *Journal of Physical Oceanography*, 28(9), 1832–1852. [https://doi.org/10.1175/1520-0485\(1998\)028<1832:OTOSLS>2.0.CO;2](https://doi.org/10.1175/1520-0485(1998)028<1832:OTOSLS>2.0.CO;2)
- Vallis, G. K. (2017). *Atmospheric and oceanic fluid dynamics*. Cambridge University Press.
- Virtanen, P., Gommers, R., Oliphant, T. E., Haberland, M., Reddy, T., Cournapeau, D., Burovski, E., Peterson, P., Weckesser, W., Bright, J., van der Walt, S. J., Brett, M., Wilson, J., Millman, K. J., Mayorov, N., Nelson, A. R. J., Jones, E., Kern, R., Larson, E., ... SciPy 1.0 Contributors. (2020). SciPy 1.0: Fun-

- damental Algorithms for Scientific Computing in Python. *Nature Methods*, 17, 261–272. <https://doi.org/10.1038/s41592-019-0686-2>
- Walin, G. (1982). On the relation between sea-surface heat flow and thermal circulation in the ocean. *Tellus*, 34(2), 187–195. <https://doi.org/10.1111/j.2153-3490.1982.tb01806.x>
- Whitworth, T. (1980). Zonation and geostrophic flow of the Antarctic circumpolar current at Drake Passage. *Deep Sea Research Part A. Oceanographic Research Papers*, 27(7), 497–507. [https://doi.org/10.1016/0198-0149\(80\)90036-9](https://doi.org/10.1016/0198-0149(80)90036-9)
- Wilson, E. A., Riser, S. C., Campbell, E. C., & Wong, A. P. S. (2019). Winter Upper-Ocean Stability and Ice–Ocean Feedbacks in the Sea Ice–Covered Southern Ocean. *Journal of Physical Oceanography*, 49(4), 1099–1117. <https://doi.org/10.1175/JPO-D-18-0184.1>
- Wolfe, C. L., & Cessi, P. (2010). What Sets the Strength of the Middepth Stratification and Overturning Circulation in Eddying Ocean Models? *Journal of Physical Oceanography*, 40(7), 1520–1538. <https://doi.org/10.1175/2010JPO4393.1>
- Wolfe, C. L., & Cessi, P. (2014). Salt Feedback in the Adiabatic Overturning Circulation. *Journal of Physical Oceanography*, 44(4), 1175–1194. <https://doi.org/10.1175/JPO-D-13-0154.1>
- You, Y. (2002). A global ocean climatological atlas of the Turner angle: Implications for double-diffusion and water-mass structure. *Deep Sea Research Part I: Oceanographic Research Papers*, 49(11), 2075–2093. [https://doi.org/10.1016/S0967-0637\(02\)00099-7](https://doi.org/10.1016/S0967-0637(02)00099-7)
- Yu, L., & Weller, R. A. (2007). Objectively Analyzed Air–Sea Heat Fluxes for the Global Ice-Free Oceans (1981–2005). *Bulletin of the American Meteorological Society*, 88(4), 527–540. <https://doi.org/10.1175/BAMS-88-4-527>
- Zahariev, K., & Garrett, C. (1997). An Apparent Surface Buoyancy Flux Associated with the Nonlinearity of the Equation of State. *Journal of Physical Oceanography*, 27(2), 362–368. [https://doi.org/10.1175/1520-0485\(1997\)027<0362:AASBFA>2.0.CO;2](https://doi.org/10.1175/1520-0485(1997)027<0362:AASBFA>2.0.CO;2)